Cell-specific expression of the transcriptional regulator RHAMM provides a timing mechanism that controls appropriate wound re-epithelialization

Received for publication, July 12, 2019, and in revised form, February 27, 2020 Published, Papers in Press, March 12, 2020, DOI 10.1074/jbc.RA119.010002

Cornelia Tolg[‡], Muhan Liu[‡], Katelyn Cousteils[§], Patrick Telmer[‡], Khandakar Alam[‡], Jenny Ma[‡], Leslie Mendina[‡], James B. McCarthy[¶], Vincent L. Morris[‖], and Eva A. Turley[‡1]**

*From the [‡]London Regional Cancer Program, London Health Sciences Centre, Victoria Hospital, London, Ontario N6A 4L6, Canada, the [¶]Department of Laboratory Medicine and Pathology, Masonic Cancer Center, Minneapolis, Minnesota 55455, the [§]Department of Biochemistry, Western University, London, Ontario N6A 5C1, Canada, the [‖]Department of Microbiology and Immunology, Western University, London, Ontario N6A 3K7, Canada, and the **Departments of Oncology, Biochemistry, and Surgery, Schulich School of Medicine, Western University, London, Ontario N6A 5C1, Canada*

Edited by Phyllis I. Hanson

Prevention of aberrant cutaneous wound repair and appropriate regeneration of an intact and functional integument require the coordinated timing of fibroblast and keratinocyte migration. Here, we identified a mechanism whereby opposing cell-specific motogenic functions of a multifunctional intracellular and extracellular protein, the receptor for hyaluronan-mediated motility (RHAMM), coordinates fibroblast and keratinocyte migration speed and ensures appropriate timing of excisional wound closure. We found that, unlike in WT mice, in *Rhamm*-null mice, keratinocyte migration initiates prematurely in the excisional wounds, resulting in wounds that have re-surfaced before the formation of normal granulation tissue, leading to a defective epidermal architecture. We also noted aberrant keratinocyte and fibroblast migration in the *Rhamm*-null mice, indicating that RHAMM suppresses keratinocyte motility but increases fibroblast motility. This cell context–dependent effect resulted from cell-specific regulation of extracellular signal-regulated kinase 1/2 (ERK1/2) activation and expression of a RHAMM target gene encoding matrix metalloprotease 9 (MMP-9). In fibroblasts, RHAMM promoted ERK1/2 activation and MMP-9 expression, whereas in keratinocytes, RHAMM suppressed these activities. In keratinocytes, loss of RHAMM function or expression promoted epidermal growth factor receptor–regulated MMP-9 expression via ERK1/2, which resulted in cleavage of the ectodomain of the RHAMM partner protein CD44 and thereby increased keratinocyte motility. These results identify RHAMM as a key factor that integrates the timing of wound repair by controlling cell migration.

The efficient and robust repair of cutaneous injury is critically important for the health and survival of organisms. In adult mammals, cutaneous wounds repair quickly to restore barrier functions, which occur in distinct and timed phases with each phase preparing the wound for the subsequent steps necessary to restore function (1–6). Key steps of repair are mesenchymal cell infiltration, deposition, and remodeling of a collagen-rich provisional extracellular matrix (ECM)[2] followed by resurfacing of the wound by keratinocytes, which migrate over and divide on the provisional matrix to re-establish a protective surface barrier. Temporal control of these repair steps is essential for restoration of cutaneous function and their dysregulation results in aberrant repair. For example, either inhibiting or stimulating keratinocyte migration (3, 7–12) or proliferation (13) following excisional skin injury can modify wound inflammation and alter dermal cell differentiation, wound contraction, and remodeling (8, 14–16). However, the molecular nature of the factors that fine-tune migration speeds or proliferation rates in order to achieve appropriate timing of repair is not well-understood. As an example, dermal fibroblasts populate cutaneous wounds prior to the initiation of keratinocyte migration, yet fibroblast motility speed is severalfold slower than keratinocytes (17, 18).

Because the creation of a wound gap is expected to release contact inhibition of motility and proliferation for both cell types (10, 19–24), it is likely that factors, which restrain keratinocyte migration and proliferation, are produced to allow time for fibroblasts to repopulate the early wound site prior to re-epithelialization.

RHAMM (gene name *HMMR*) is a multifunctional intracellular and extracellular protein whose expression is normally

This work was supported by Lawson Health Sciences Center discretionary fund (to E. T.), the Breast Cancer Society of Canada (to E. T.), and the Chairman's Fund in Cancer Research and the Elsa-Pardee Foundation (to J. B. M.). The authors declare that they have no conflicts of interest with the contents of this article.

This article contains Fig. S1.

[1] To whom correspondence should be addressed: London Regional Cancer Program, London Health Sciences Centre, Victoria Hospital, London, Ontario N6A 4L6, Canada. E-mail: Eva.Turley@lhsc.on.ca.

[2] The abbreviations used are: ECM, extracellular matrix; RHAMM, receptor for hyaluronan-mediated motility; MMP-9, matrix metalloprotease 9; EGF, epidermal growth factor; EGFR, epidermal growth factor receptor; ERK, extracellular signal-regulated kinase; qRT-PCR, quantitative RT-PCR; BisTris, 2-[bis(2-hydroxyethyl)amino]-2-(hydroxymethyl)propane-1,3-diol; ddH_2O, double distilled H_2O; DAPI, 4′,6-diamidino-2-phenylindole; GAPDH, glyceraldehyde-3-phosphate dehydrogenase; DMEM, Dulbecco's modified Eagle's medium; FBS, fetal bovine serum; HRP, horseradish peroxidase; PDGF, platelet-derived growth factor; MAP, mitogen-activated protein; MEK, mitogen-activated protein kinase/extracellular signal-regulated kinase kinase; Ab, antibody; EMEM, Eagle's minimal essential medium; DAB, 3,3′-diaminobenzidine; FW, forward; RV, reverse; RITC, rhodamine B-isothiocyanate; PAR3, partitioning defective protein 3.

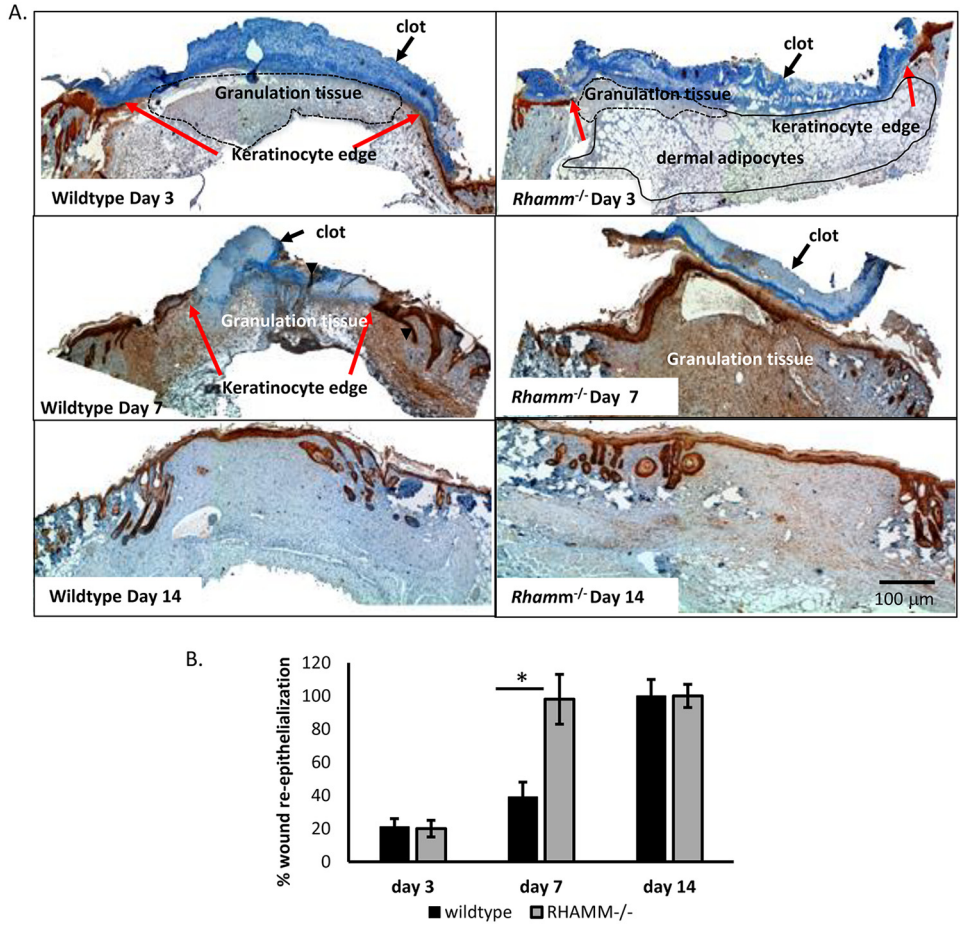

Figure 1. *Rhamm*$^{-/-}$ keratinocytes re-surface excisional skin wounds more rapidly than WT comparators. *A,* cross-sections of the center of excisional skin wounds were stained for pan-keratin (*brown*) and counterstained with hematoxylin. *Red arrows* indicate the leading edge of the migrating keratinocyte layer. *Dotted black lines* in day 3 images outline the underlying granulation tissue, and the *black arrow* indicates the clot. Subcutaneous fat (labeled dermal adipocytes) has uniquely expanded into the granulation tissue of *Rhamm*$^{-/-}$ mice. *Rhamm*$^{-/-}$ wounds are delayed in granulation tissue formation, but resurfacing of wounds by keratinocytes is accelerated relative to WT wounds. *B,* quantification of wound re-epithelialization shows that *Rhamm*$^{-/-}$ wounds have completed re-surfacing by day 7, and WT wounds complete this process by day 14. Values are the mean and S.E. $n = 3$ mice. *, $p < 0.01$.

restricted to repairing tissues (25–28). Intracellular RHAMM regulates gene expression through association with transcriptional complexes (29) and centrosome/mitotic spindle stability through its association with proteins such as TPX2, AURKA, and BRCA1 (30, 31). These intracellular functions are linked to regulation of cell proliferation. Extracellular (cell surface) RHAMM binds to hyaluronan and performs co-receptor signaling functions through CD44, other hyaluronan receptors, and growth factor receptors such as PDGF (26, 32). RHAMM is transiently expressed during the inflammation (25, 26, 28, 33, 34) and granulation tissue stages of excisional injury (35, 36). RHAMM signaling functions are required for macrophage and fibroblast migration in response to tissue injury, and genomic deletion of this gene reduces both innate immune cell influx/function and fibroplasia during repair (33, 35). In addition to its role in cell migration, RHAMM also regulates transition through the G_2M phase of the cell cycle (30, 37) predicting a role for this protein in controlling the cellular proliferation needed for tissue repair. RHAMM is expressed in macrophages, fibroblasts, and wound-edge keratinocytes during the early stages of excisional repair when macrophages and fibroblasts are migrating into the wound site but is unexpectedly strongly reduced when keratinocytes initiate migration over granulation tissue (35). These observations prompted us to assess whether the motogenic and mitogenic signaling functions of RHAMM are cell context–dependent. Here, we compare the consequences of RHAMM-loss on the migration and proliferation of dermal fibroblasts and keratinocytes and provide evidence for a role of RHAMM in orchestrating the temporal coordination of wound repair by stimulating fibroblast migration but restraining this function in keratinocytes. We further identify cell context–dependent mechanisms responsible for these opposing effects of RHAMM.

Results

Rhamm-loss results in aberrant epidermal architecture and alters the timing of wound re-epithelialization

Granulation tissue is detected in excisional wounds of WT mice by day 3, and keratinocyte migration is initiated at the wound edge by day 7 (Fig. 1*A*). Re-epithelialization is complete by day 14 (Fig. 1*B*). In contrast, *Rhamm*$^{-/-}$ wounds produce very little granulation tissue by day 3 and have expanded a large depot of dermal adipocytes, which is lost by day 7 (Fig. 1*A*).

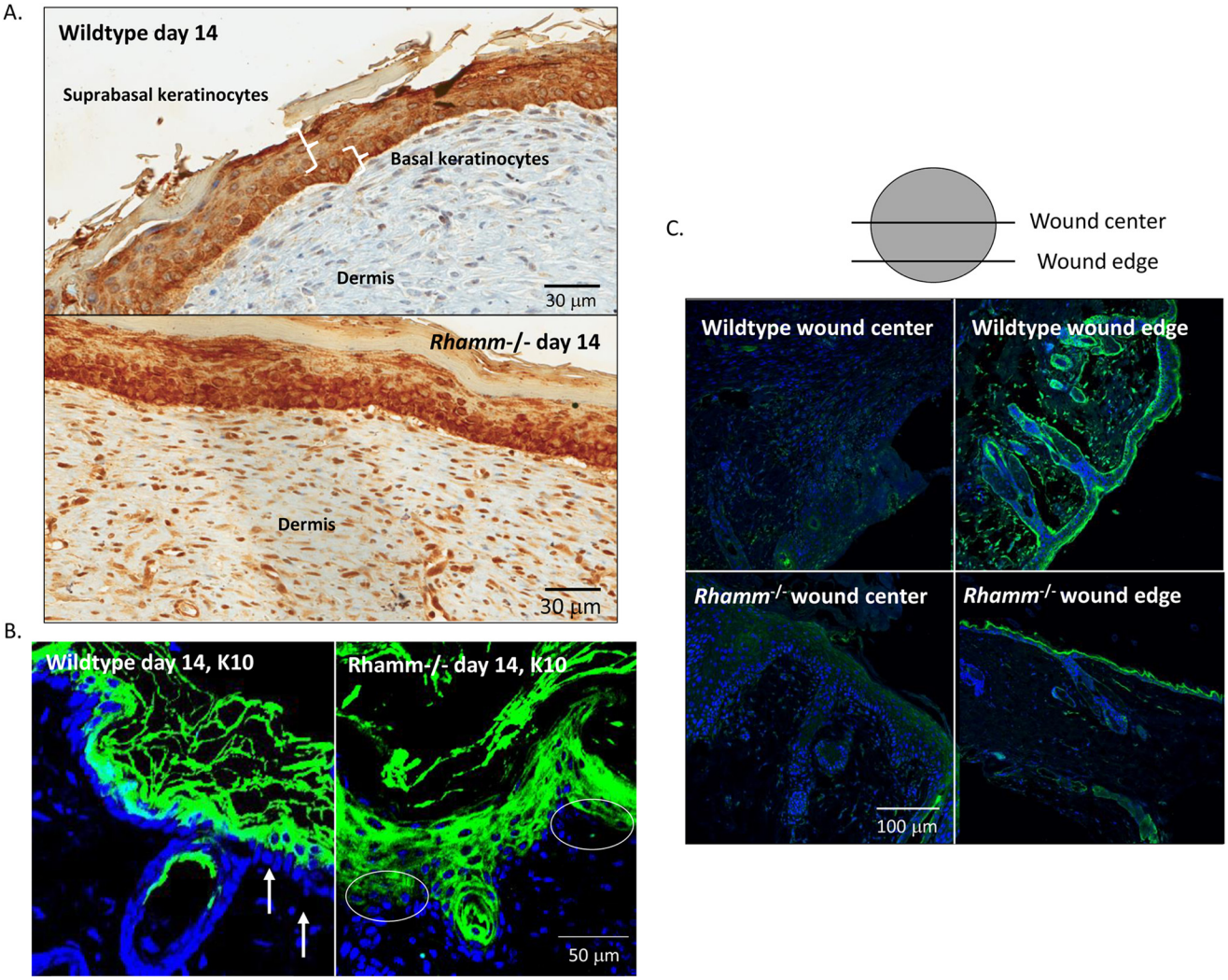

Figure 2. *Rhamm*-loss causes aberrant epidermal differentiation. *A,* cross-sections of WT and *Rhamm*$^{-/-}$ excisional skin wounds at day 14 post-wounding were stained for pan-keratin and show that WT epidermis has re-organized into discernable basal, suprabasal, and cornified layers by day 14; however, these layers are not distinguishable in *Rhamm*$^{-/-}$ epidermis. *B,* cytokeratin 10 (K10) staining of day 14 *Rhamm*$^{-/-}$ and WT wounds was used to identify the suprabasal keratinocyte layer. *C,* Par3 expression was detected by immunohistochemistry and used as an epidermal polarization marker. Loss of RHAMM reduces expression of this protein at day 14 wound centers and edges.

Migration of keratinocytes is initiated at the wound edge by day 3 when the dermal microenvironment is aberrant. *Rhamm*$^{-/-}$ wound re-surfacing by keratinocytes is more rapid than in the WT comparator and is completed by day 7 (Fig. 1*B*). Although WT keratinocytes have organized into identifiable basal and supra-basal layers by day 14, *Rhamm*$^{-/-}$ keratinocytes are disorganized with no clear histological basal/supra-basal demarcation (Fig. 2*A*). This lack of epidermal polarity resulting from *Rhamm*-loss is confirmed by aberrant expression of keratin 10 and the Partitioning defective protein 3 (PAR) polarity complex (38), detected by PAR staining (Fig. 2, *B* and *C*). The boundary between basal and suprabasal keratinocytes is clearly demarked in WT wounds by suprabasal keratin 10 staining (Fig. 2*B*) and strong PAR staining in basal keratinocytes (Fig. 2*C*). In contrast, all keratinocyte layers of the day 14 *Rhamm*$^{-/-}$ wound are keratin 10–positive (Fig. 2*B*), and PAR is poorly expressed throughout the epidermis (Fig. 2*C*).

Collectively, these results confirm that *Rhamm*-loss alters mesenchymal differentiation and delays granulation tissue formation, as reported previously (35, 39). It also identifies a novel effect on re-epithelialization and epidermal re-modeling.

RHAMM protein expression is transient but ubiquitous in excisional wounds

We have previously shown that RHAMM mRNA expression is undetectable in homeostatic skin but is transiently expressed between days 1 and 7 in excisional wounds (35). To facilitate identification of mechanism(s) for increased re-epithelialization of *Rhamm*$^{-/-}$ wounds, the localization of RHAMM protein in excisional wounds was assessed using immunohistochemistry (Fig. 3*A*). This analysis confirmed the transient expression of RHAMM and showed that protein expression is maximum on day 1 after excisional wounding and is ubiquitously expressed at the wound edge in all skin layers. Staining is gradually reduced between days 3 and 14, raising the possibility that RHAMM may suppress keratinocyte functions involved in re-epithelialization, and loss of expression releases this inhibition. Positive staining for RHAMM in the epidermis was con-

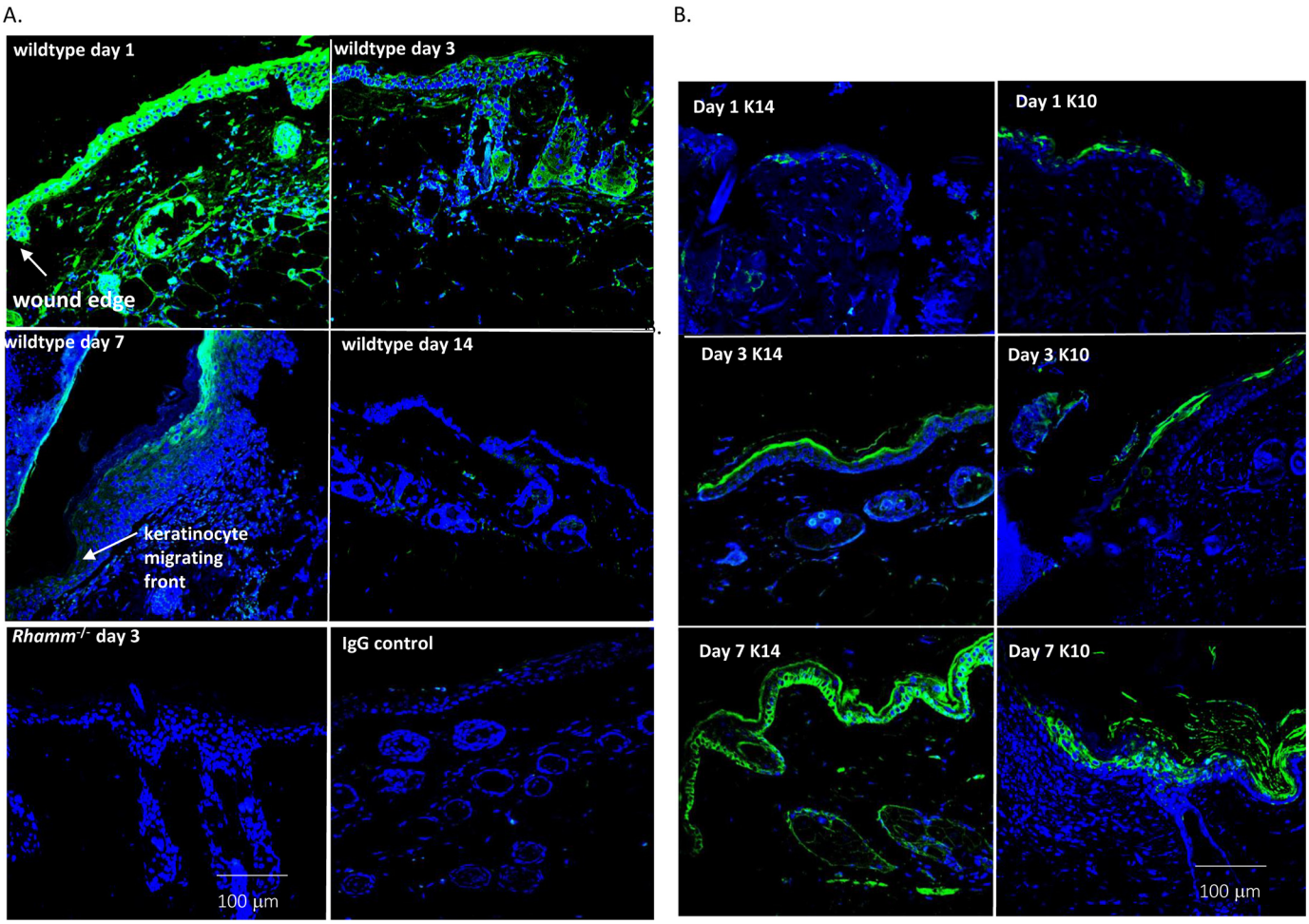

Figure 3. RHAMM protein is transiently expressed in excisional wounds. *A,* strong RHAMM staining appears in wounds and peri-wound areas at day 1 post-excisional injury and occurs in all skin layers. By day 3, staining intensity has notably decreased in the interfollicular epidermis and is absent by day 14. *White arrows* indicate the wound edge. Staining is negative in *Rhamm*$^{-/-}$ wounds (day 3 at wound edge shown) to show antibody specificity for RHAMM. *B,* cytokeratin 10 (K10) and cytokeratin 14 (K14) staining of day 1, 3, and 7 WT wounds.

firmed by identifying keratinocytes with the markers keratin 10 and 14 (Fig. 3*B*). Notably, RHAMM expression is highest when keratin 10 and 14 expression is low. As RHAMM expression disappears, keratin 10 and 14 staining becomes stronger (Fig. 3*B*). We have previously shown that RHAMM is also expressed in fibroblasts and macrophages of excisional skin wounds (35).

Aberrant re-epithelialization and dermal fibroplasia of excisional wounds can result from de-regulated cell migration and/or proliferation (22, 40). Because intracellular RHAMM affects centrosome/mitotic spindle stability and cell-surface RHAMM regulates progression through the cell cycle (30), we first assessed the consequences of its expression-loss on fibroblast and keratinocyte proliferation.

Rhamm-loss has no detectable effect on keratinocyte and fibroblast proliferation

Quantification of Ki67 staining in the epidermis (Fig. 4*A*) and dermis (Fig. 4*B*), when active proliferation occurs in both compartments, revealed no significant difference between *Rhamm*$^{-/-}$ fibroblasts or keratinocytes compared with WT counterparts ($p > 0.05$). To further assess this, *Rhamm*$^{-/-}$ and Rhamm-rescued dermal fibroblasts were cultured. Re-expressed RHAMM was confirmed by immunoblot analysis (Fig. 4*C*). No difference in staining for the proliferation marker Ki67 was observed (Fig. 4*D*). To address the effect of cell-surface RHAMM function-loss in keratinocytes, in particular that of cell-surface RHAMM, a human keratinocyte line, HaCaT, was used. These cells express RHAMM protein (Fig. 4*C*). A function blocking RHAMM antibody has no effect on the proliferation of these keratinocytes (Fig. 4*E*), mirroring the lack of effect of *Rhamm*-loss on keratinocyte proliferation observed *in vivo*. Because differences in proliferation do not account for the effect of Rhamm-loss on excisional repair, we next investigated the consequence of this loss on cellular migration.

Rhamm-loss suppresses fibroblast motility but promotes this function in keratinocytes

Rhamm-loss alters the migration properties of both primary keratinocyte and fibroblast migration in culture (Figs. 5–8). As we have reported previously (35), deletion of *Rhamm* in fibroblasts reduces their migration (Fig. 5). Both the migration speed and net translocation of immortalized Rhamm-rescued fibroblasts are significantly greater than *Rhamm*$^{-/-}$ counterparts (Fig. 5, *A* and *B*). However, migration persistence of these cells is not affected by *Rhamm*-loss (Fig. 5*C*). The migration velocity of primary WT dermal fibroblasts is also more rapid than

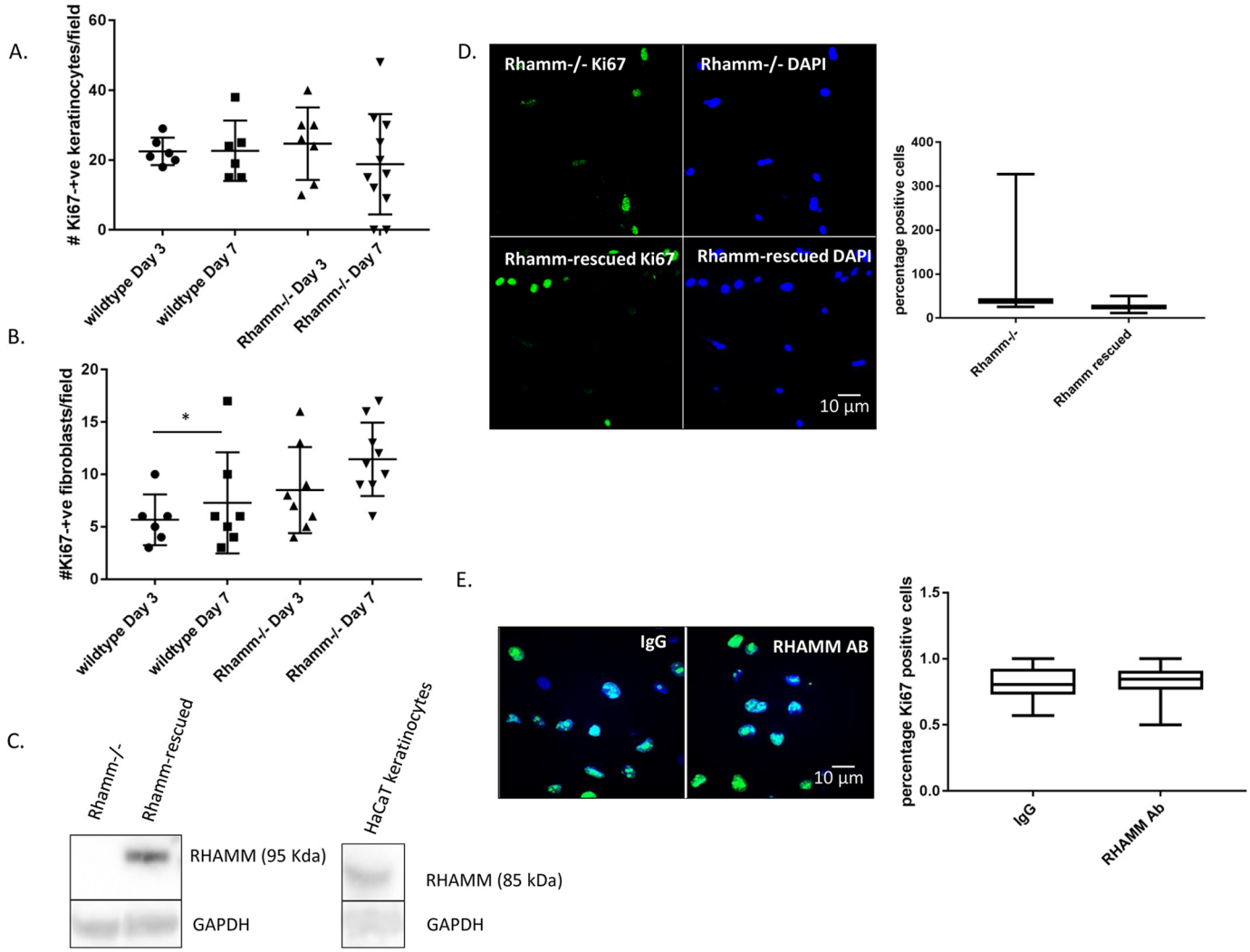

Figure 4. *Rhamm*-loss does not alter keratinocyte or fibroblast proliferation. Cell proliferation was quantified using Ki67 immunohistochemistry (*A–C*). *A* and *B*, Ki67 staining of keratinocytes (*A*) or dermal fibroblasts (*B*) of day 3 and 7 wound tissue sections is not significantly different in WT *versus* $Rhamm^{-/-}$ mice. Values are the mean and S.E. $n = 50$ cells/3 mice, $p > 0.05$. *C*, Western blot analysis of RHAMM expression in HaCaT keratinocytes and fibroblasts. *D*, *Rhamm*-loss ($Rh^{-/-}$) also did not significantly alter cell survival/proliferation of fibroblasts compared with WT as detected by Ki67 staining. *Box* and *whisker plots* of $n = 50$ cells, $p > 0.05$. *E*, function-blocking RHAMM antibody did not significantly change Ki67 staining of HaCaT keratinocytes in culture. *Box* and *whisker plots* of $n = 100$ cells, $p > 0.05$.

$Rhamm^{-/-}$ counterparts (Fig. 5*D*). The function-blocking antibody, which was used to assess cell proliferation in keratinocytes, significantly inhibits motility speed of WT fibroblasts but does not significantly alter $Rhamm^{-/-}$ motility speed. Collectively, these results indicate that dermal fibroblasts are dependent on RHAMM expression for motility speed and net translocation.

Unexpectedly, *Rhamm*-loss increases rather than decreases keratinocyte migration (Figs. 6–8). We first compared the migration properties of primary WT and $Rhamm^{-/-}$ keratinocytes responding to EGF. EGF is the major motogenic cytokine that promotes re-epithelialization in excisional wounds. Both the migration velocity (Fig. 6, *A* and *B*) and net translocation of keratinocytes (Fig. 6, *C* and *D*) are increased by *Rhamm*-loss. Directional persistence is unaffected by Rhamm-loss (Fig. 7, *B* and *C*). Blocking RHAMM cell-surface signaling with the RHAMM antibody also increases migration speed of WT keratinocytes (Fig. 8, *A* and *B*). The specificity of this antibody for RHAMM protein is demonstrated by its lack of effect on $Rhamm^{-/-}$ keratinocyte migration speed (Fig. 8, *C* and *D*). Collectively, these results show that the motogenic effect of RHAMM expression is cell-type–dependent because it promotes fibroblast motility but inhibits this function in keratinocytes.

Temporal regulation of motogenic and mitogenic signaling cascades such as the MAP kinases controls appropriate migration necessary for normal wound repair (41–43). We have previously shown that RHAMM-induced fibroblast migration requires ERK1/2 activity (31), and we confirm this finding here (Fig. 5*D*). We therefore next investigated whether RHAMM also regulates activity of these kinases in keratinocytes. To facilitate these analyses, we utilized a keratinocyte cell line (HaCaT). These cells express RHAMM (Fig. 4*C*), and the RHAMM antibody significantly increases their migration velocity in scratch-wound assays (Fig. 9, *A* and *B*) and random motility (Fig. 9*C*), confirming a role for cell-surface RHAMM signaling in regulating migration of this immortalized keratinocyte line.

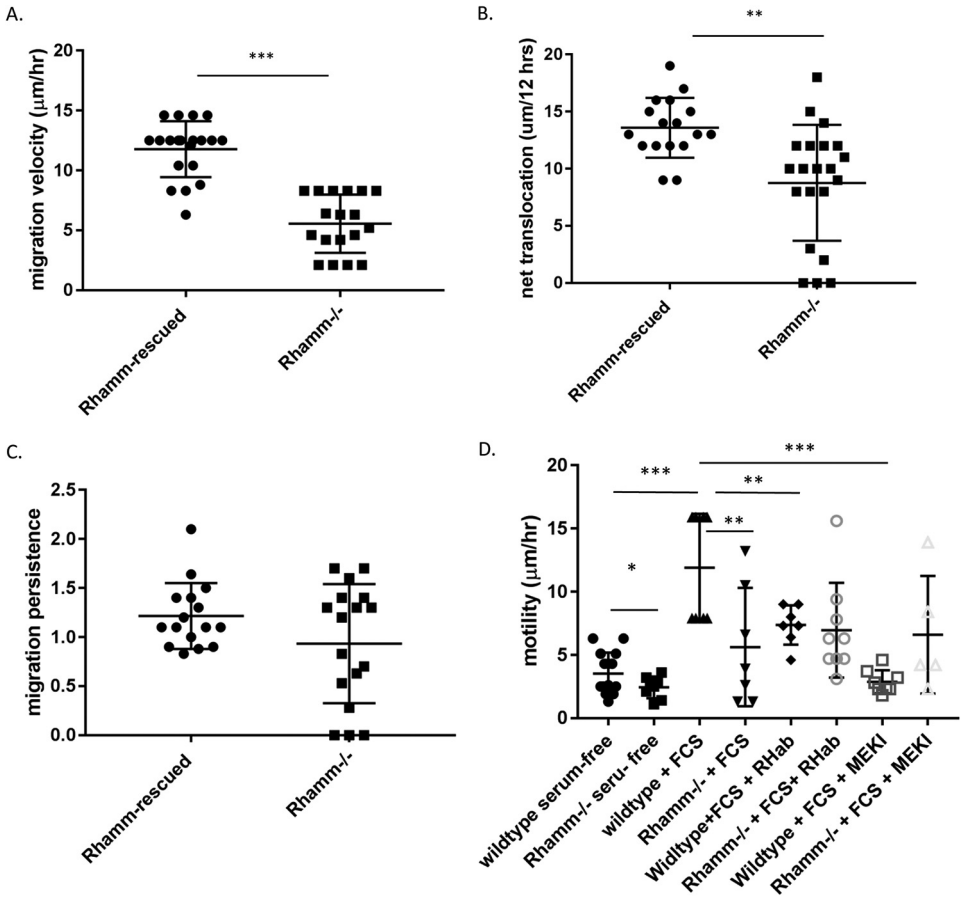

Figure 5. *Rhamm*-loss reduces fibroblast migration. Immortalized Rhamm$^{-/-}$ fibroblasts were transfected with a full-length mouse *Rhamm* cDNA, and motility of the null and rescued cells was quantified. Rescue of *Rhamm*$^{-/-}$ fibroblasts significantly increases cell motility velocity (*A*) and net translocation (*B*) but migration persistence is not affected (*C*). *D,* speed of WT fibroblasts that express RHAMM is significantly greater than *Rhamm*$^{-/-}$ counterparts in defined medium. WT fibroblast migration is increased by fetal calf serum (*FCS*) and is strongly reduced by either a RHAMM function–blocking antibody or MEK inhibitor. *Rhamm*$^{-/-}$ fibroblasts are unresponsive to these stimuli and inhibitors. Results are shown as scatter plots. *, $p < 0.05$; **, $p < 0.01$; and ***, $p < 0.001$.

Rhamm-loss alters temporal regulation of wound ERK1/2 activity

Immunohistochemical analyses of excisional wounds *in vivo* show that the levels of active ERK1/2, detected by nuclear phospho-ERK1/2 (p-ERK1/2), are higher in keratinocytes of *Rhamm*$^{-/-}$ *versus* WT wounds between days 3 and 14 post-excisional injury (Fig. 10, *A* and *B*). By day 14, p-ERK1/2 staining is largely restricted to basal keratinocytes in WT wounds (Fig. 10*A*). At this time point, strongly p-ERK1/2–positive *Rhamm*$^{-/-}$ keratinocytes occur throughout a multilayered, disorganized epidermis that does not have a clear basal layer. These results predict that RHAMM expression suppresses ERK1/2 activity, which loss of *Rhamm* releases, and that this may impact both keratinocyte migration and differentiation. Cell cultures were therefore utilized to directly assess a role of ERK1/2 activation in RHAMM-regulated keratinocyte migration.

Cultured keratinocytes and fibroblasts are dependent on ERK1/2 activity for motility and RHAMM regulates this activity

We have previously reported that RHAMM expression promotes growth factor-regulated ERK1/2 activity in fibroblasts and that these MAP kinases are required for RHAMM-dependent fibroblast motility (35). These previous results are confirmed here. RHAMM expression does not affect basal levels of ERK1/2 activity but increase and prolong activation of these MAP kinases in response to PDGF (Fig. S1). Inhibition of the upstream kinase MEK suppresses migration of fibroblasts expressing RHAMM but has no significant effect on *Rhamm*$^{-/-}$ comparators (Fig. 5*D*). As observed *in vivo*, p-ERK1/2 levels are significantly higher in cultured primary *Rhamm*$^{-/-}$ *versus* WT keratinocytes (Fig. 10*C*). Furthermore, blocking ERK1/2 activity with a MEK inhibitor strongly decreases migration velocity of *Rhamm*$^{-/-}$ keratinocytes (Fig. 10*D*). Because keratinocytes are migrating in response to EGF, we next investigated the relationship among EGFR, RHAMM, and ERK1/2 in RHAMM-regulated keratinocyte migration using the HaCaT cell line.

Extracellular RHAMM blocks EGFR motogenic signaling through ERK1/2

We first confirmed that RHAMM antibody–stimulated HaCaT migration in response to EGF is inhibited by blocking EGFR signaling (Fig. 11*A*). Because EGFR-stimulated ERK1/2 activity is required for keratinocyte migration (44), we next confirmed that blocking cell-surface RHAMM alters ERK1/2 activity. As shown in immunoblot assays, the RHAMM antibody increases phospho-ERK1/2 in HaCaT keratinocytes (Fig.

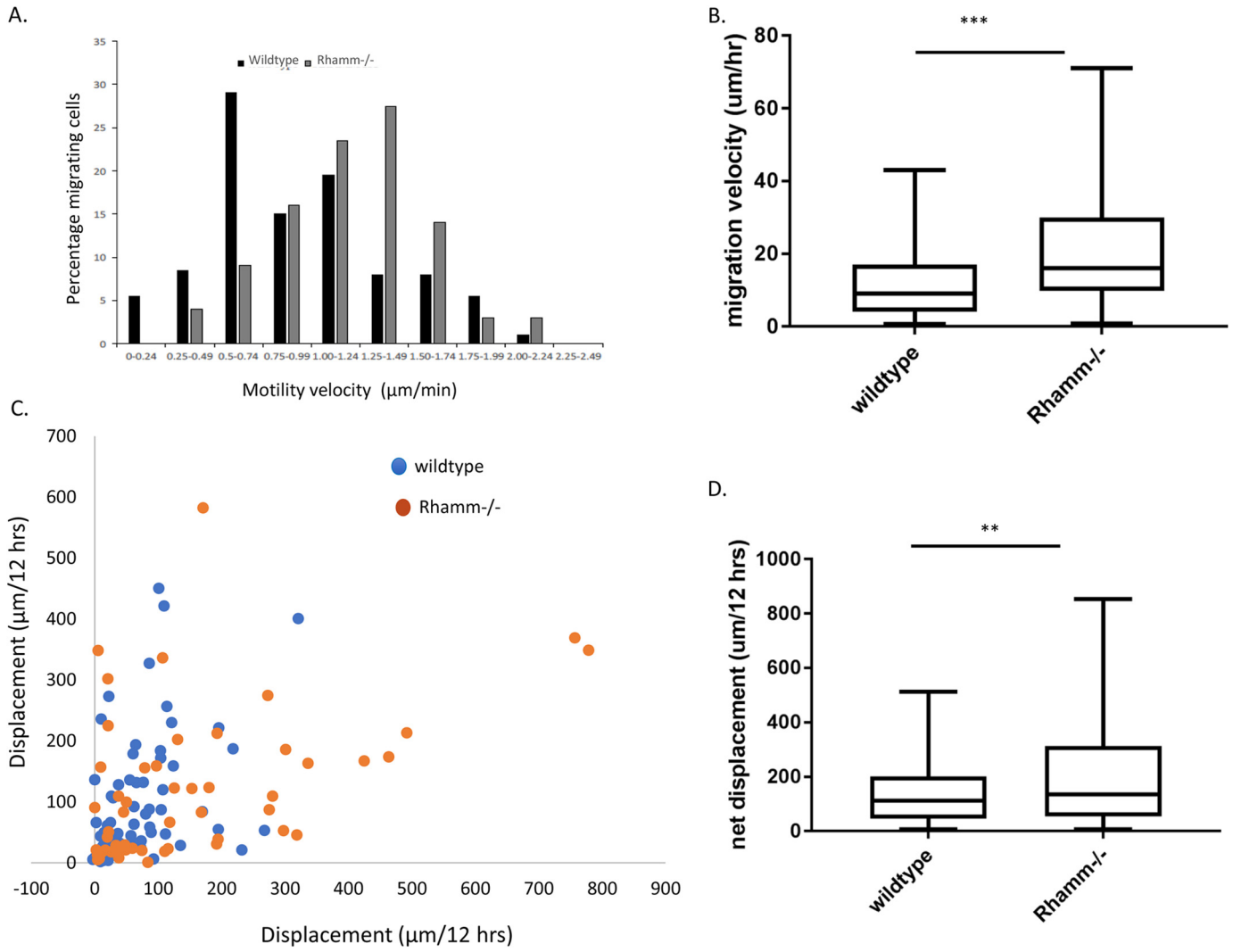

Figure 6. *Rhamm*-loss promotes keratinocyte migration. *A–D, Rhamm*$^{-/-}$ primary keratinocytes migrate more rapidly than WT counterparts in random migration assays. Primary keratinocytes were isolated from *Rhamm*$^{-/-}$ or WT 1–2-day-old mouse pups, and migration was stimulated by EGF. *A,* velocity range distribution of WT or *Rhamm*$^{-/-}$ keratinocytes: $n = 64$ cells/assay, $n = 2$ assays, *B,* velocity of WT and *Rhamm*$^{-/-}$ keratinocytes. *Box* and *whisker* plots of $n = 64$ cells. *C,* displacement plot of individual WT and *Rhamm*$^{-/-}$ keratinocytes. *D, Box* and *whisker plot* showing net displacement of WT and *Rhamm*$^{-/-}$ keratinocytes. $n = 50$ cells. **, $p < 0.01$; ****, $p < 0.001$.

11*B*). Furthermore, RHAMM antibody–stimulated HaCaT migration requires ERK1/2 activity because inhibition of MEK1 blocks this increase (Fig. 11*C*). These results confirm a role for EGFR and ERK1/2 activity in the migration of HaCaT keratinocytes stimulated by blocking cell-surface RHAMM. We therefore next assessed the association of RHAMM with EGFR and the consequences of blocking cell-surface RHAMM on EGFR activation. Immunostaining shows that EGFR and RHAMM are co-localized in a subset of HaCaT keratinocytes and that the RHAMM antibody significantly reduces this association (Fig. 11*D*). However, the RHAMM antibody did not result in detectable changes in EGFR activity as detected by phosphorylation status (Fig. 11*E*). These results suggest that RHAMM dissociation from EGFR affects ERK1/2-dependent motility downstream of EGFR activation. We therefore next analyzed ERK1/2-dependent motogenic gene expression in keratinocytes and fibroblasts.

MMP-9 activity is required for migration of keratinocytes and fibroblasts

To identify motogenic genes that are differentially regulated by RHAMM in keratinocytes and fibroblasts, focused PCR arrays for motility-associated genes were performed (Fig. 12) for primary mouse keratinocytes. Results of these arrays were compared with results from unbiased Affymetrix microarrays of serum-stimulated fibroblasts. Significant gene-expression changes result from *Rhamm*-loss in keratinocytes (Fig. 12*A*) and fibroblasts (Fig. 12*B*), which pathway analyses (Ingenuity Pathway Analysis) confirmed are linked to RHAMM in motility signaling ($p < 6.9E-07$). Only two genes *Mmp-9* and *Ptk2*, which are known ERK1/2 targets (45–47), are differentially affected by *Rhamm*-loss in keratinocytes *versus* fibroblasts. *Rhamm*-loss in keratinocytes increases expression of these genes in keratinocytes but decreases their expression in fibroblasts. Because MMP-9 is well-characterized to promote the motility of keratinocytes (48) and fibroblasts (49) during wound

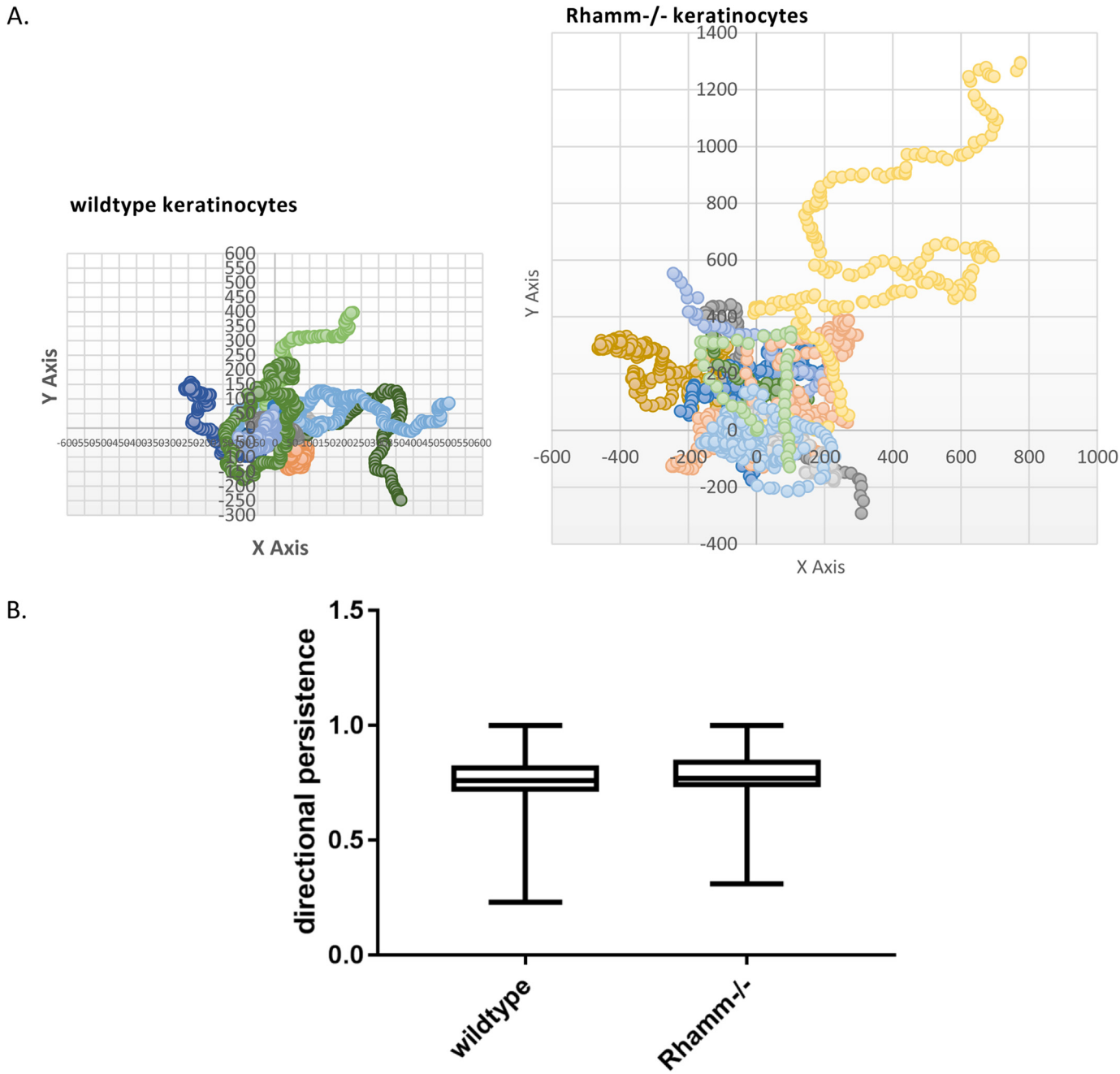

Figure 7. *Rhamm*-loss does not affect the directional persistence of keratinocyte migration. The directional persistence of primary WT and *Rhamm*$^{-/-}$ keratinocytes was calculated as the total translational/net translocation. *Rhamm*$^{-/-}$ keratinocytes did not detectably differ from WT comparators in this motility function. *A,* diagram of time-lapse analyses of individual keratinocytes. *B*, *box* and *whisker plot* of each time point shown in *A*.

repair, the role of this metalloproteinase in RHAMM-regulated migration was further investigated.

The changes in *Mmp-9* mRNA expression in *Rhamm*$^{-/-}$ keratinocytes and fibroblasts detected by PCR arrays were first confirmed with qRT-PCR (Fig. 13, *A* and *B*), and the dependence of *Mmp-9* expression on ERK1/2 activity in these two cell types was confirmed (Fig. 13, *A* and *B*). The dependence of fibroblasts and keratinocytes migration on Mmp-9 activity was then assessed.

An inhibitor specific for MMP-9 significantly reduces migration of HaCaT keratinocytes in response to the RHAMM antibody in the scratch-wound assays (Fig. 13*C*). The MMP-9 inhibitor also strongly blunts migration of *Rhamm*-rescued null fibroblasts (Fig. 13*D*). To confirm that RHAMM expression/function affects MMP-9 activity and that the inhibitor is specific for this metalloproteinase, zymograms using conditioned medium and *in situ* degradation assays using live cells were performed. Results show that the RHAMM antibody selectively increases MMP-9 activity (Fig. 14, *A* and *B*). Furthermore, the MMP-9 inhibitor used for migration assays is specific for this metalloproteinase (Fig. 14*B*). *In situ* degradation assays show that *Rhamm*-rescued fibroblasts significantly degrade more denatured rhodamine B-isothiocyanate (RITC)-collagen than *Rhamm*$^{-/-}$ fibroblasts and that this is blocked by the MMP-9

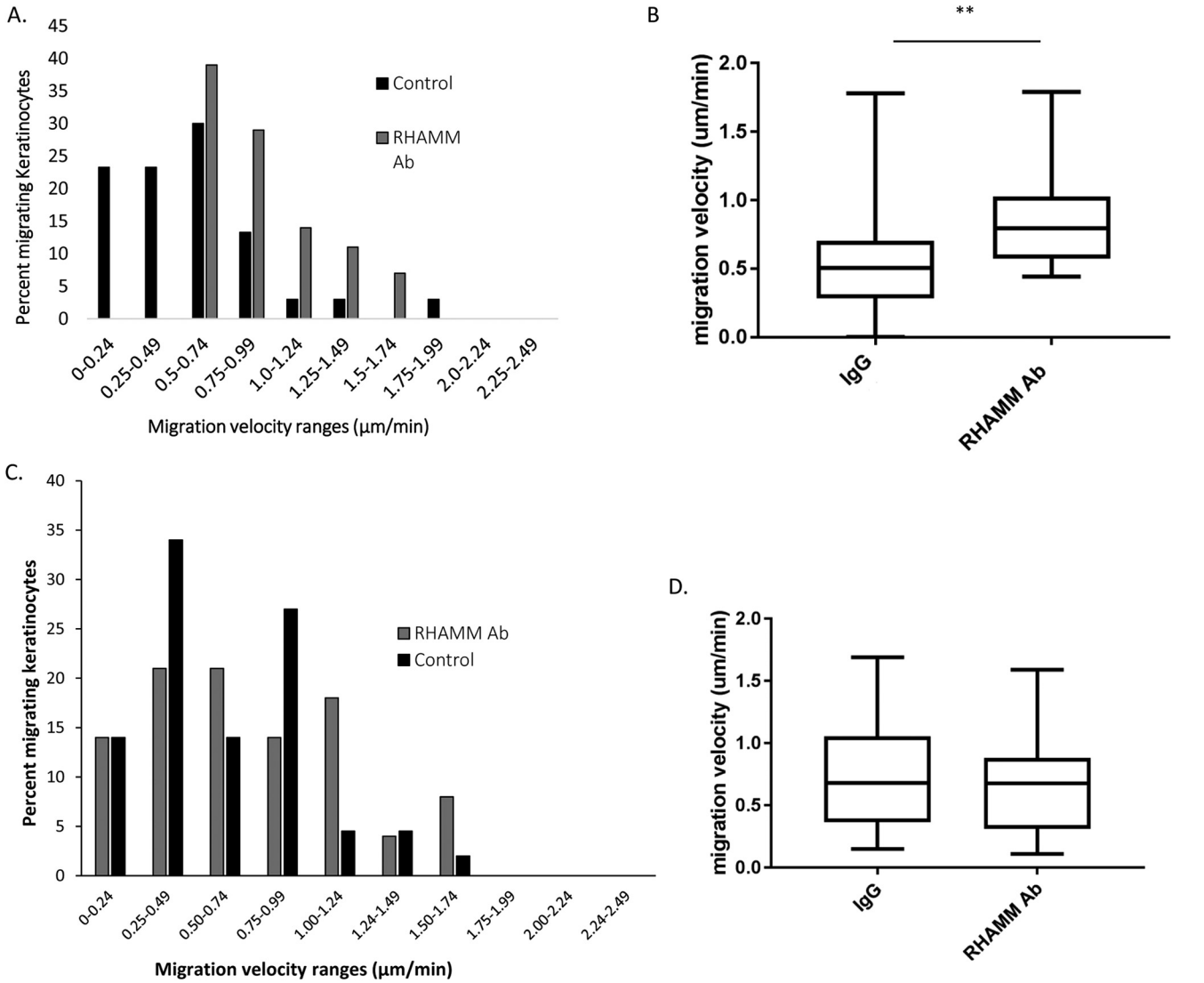

Figure 8. Blocking extracellular RHAMM with a RHAMM antibody stimulates the migration of WT keratinocytes but has no effect on *Rhamm*$^{-/-}$ keratinocytes. Primary keratinocytes were isolated from newborn mouse skin, plated onto fibronectin-coated culture surfaces in the presence of RHAMM blocking antibody or nonimmune IgG, used as a control, and then filmed. *A,* migration velocity profile of individual primary WT keratinocytes. *B, box* and *whisker plot* showing that the RHAMM antibody (*RHAMM Ab*) significantly increases WT keratinocyte motility velocity. **, $p < 0.01$. *C,* migration velocity profile of individual primary *Rhamm*$^{-/-}$ keratinocytes. *D, box* and *whisker plot* showing that the RHAMM antibody does not significantly affect the migration velocity of primary *Rhamm*$^{-/-}$ keratinocytes.

inhibitor (Fig. 14, *C* and *D*). Collectively, these results show that inhibiting RHAMM function or expression releases an EGFR/MMP-9 mechanism that supports keratinocyte migration. In contrast, gain of RHAMM function or expression activates a serum/MMP-9 mechanism that supports fibroblast migration.

Extracellular RHAMM is not an integral membrane protein but must partner with membrane-spanning proteins to affect signaling activity (35, 50–53). CD44 is one RHAMM protein partner (25–27, 54, 55), which is known to modify EGFR signaling in keratinocytes (56, 57) and serum/growth factor signaling in fibroblasts (35, 58). Co-distribution of CD44 and RHAMM has previously been shown to functionally integrate elevated migration of mesenchymal cells (26, 59, 60). Because CD44 co-distributes with EGFR on keratinocytes (61, 62) and exerts pro- or anti-migration effects depending upon the cellular and microenvironmental context (63–66), we next investigated the role of CD44 in RHAMM-regulated keratinocyte motility.

RHAMM-blocking antibody promotes MMP-9-dependent CD44 shedding

To assess a role for CD44 in RHAMM-regulated keratinocyte migration, HaCaT cells were scratch-wounded and treated with a function-blocking CD44 antibody ± RHAMM antibody or nonimmune IgG (Fig. 15*A*). Blocking CD44 function stimulated HaCaT keratinocyte migration to a similar level as blocking RHAMM function (Fig. 15*A*). Simultaneous addition of both anti-CD44 and anti-RHAMM antibodies did not further increase motility predicting that CD44 and RHAMM coordinate suppression of migration.

CD44 suppression of migration can be released by ectodomain shedding of this protein (67, 68). A number of enzymes (68), notably MMP-9 (69, 70), proteolyze CD44 prompting us to assess whether exposure of HaCaT keratinocytes to RHAMM antibodies releases CD44 and whether this requires

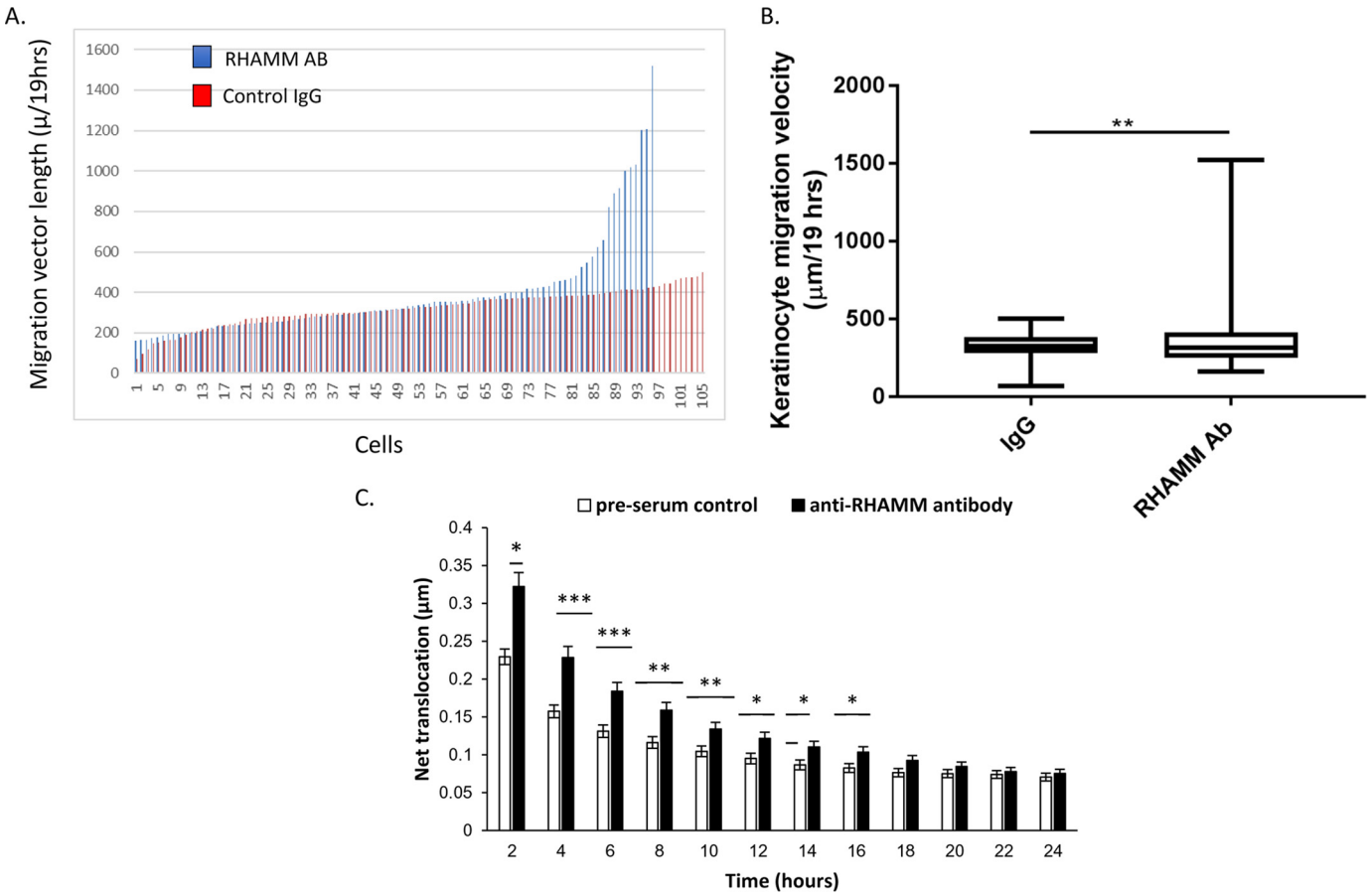

Figure 9. Blocking extracellular RHAMM with a RHAMM antibody stimulates migration of HaCaT keratinocytes. *A* and *B*, scratch wounds of HaCaT cells were treated with RHAMM antibodies or control IgG. Migration vector length over time was determined by cinemicrography. *A* shows vector length of $n = 100$ individual cells. *Graph in B* shows *box* and *whisker plots* of the results in *A*. **, $p < 0.01$. *C*, random motility net translocation of HaCaT keratinocytes treated with RHAMM antibodies or control IgG. *, $p < 0.05$; ***, $p < 0.001$.

expression and activity of MMP-9. RHAMM-blocking antibodies significantly promoted ectodomain shedding of CD44 into supernatant medium collected from HaCaT cells, as detected by an ELISA (Fig. 15*B*). Furthermore, shedding was blocked by inhibiting MMP-9 activity. Results also show that control cultures exhibit a lower level of CD44 shedding that can also be blocked by inhibiting MMP-9 activity (Fig. 15*B*). MMP-9 activity is a critical factor in releasing RHAMM- and CD44-mediated migration inhibition because addition of recombinant-active MMP-9 by itself is sufficient to significantly stimulate keratinocyte motility (Fig. 15*C*). These results show that MMP-9 expression is required to release CD44 and promote keratinocyte migration and that this is mediated by blocking extracellular RHAMM function (*e.g.* Fig. 16*A*).

Discussion

Here, we show that RHAMM expression is required for the re-formation of a polarized epidermal architecture and function following wounding. Its absence may therefore be related to wound-healing abnormalities such as keloids, diabetic ulcers, and hypertrophic scarring. RHAMM inhibits keratinocyte migration *in vivo* and *in culture,* while conversely, it stimulates dermal fibroblast migration. RHAMM is transiently-expressed by both cell types in excisional wounds when mesenchymal cells are migrating into the wound to produce a provisional matrix, and keratinocyte migration has not yet been initiated. Therefore, we propose that this opposing effect of RHAMM on cell migration is a critical factor in coordinating the timing of excisional wound re-surfacing by keratinocytes relative to in-migration of fibroblasts/mesenchymal cells so that keratinocytes migrate on the provisional matrix (Fig. 16*B*). We predict that alteration of normal coordination has long-term consequences for re-establishing appropriate epidermal architecture. Thus, *Rhamm* genomic-loss impairs the development of the basal and supra-basal layers of the epidermis, and analyses of repaired tissue show that the polarity of basal keratinocytes is not appropriately re-established. Paracrine communication among keratinocytes and dermal cells, such as fibroblasts and adipocytes, is known to be required for establishing appropriate mesenchymal differentiation and skin tissue architecture (71, 72) predicting that *Rhamm*-loss modifies this interaction. Either *Rhamm* genomic-loss or blocking extracellular RHAMM function (39) promotes premature dermal adipogenesis, and therefore $Rhamm^{-/-}$ keratinocytes migrate over an inappropriately predominant adipocyte microenvironment, which likely alters key paracrine/cytokine signals required for establishing epidermal architecture. Intracellular RHAMM functions have previously been linked to establishing epithelial polarity (73, 74), and loss of both extracellular and

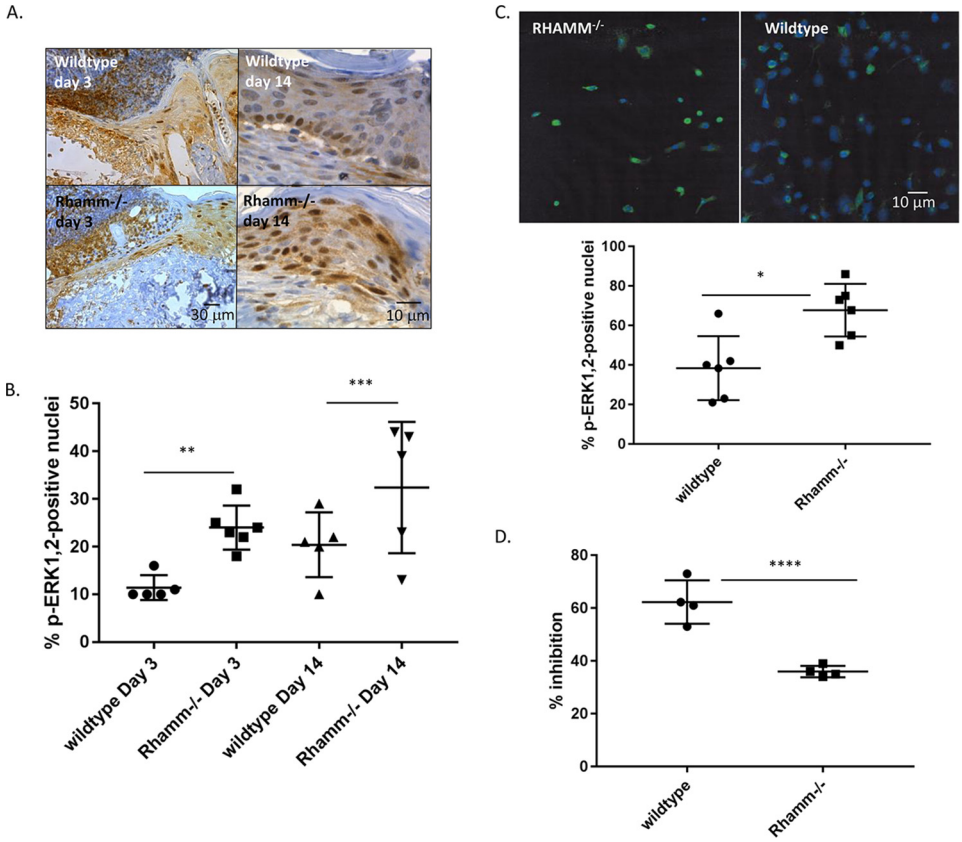

Figure 10. RHAMM suppresses ERK1/2 activity in wounds and EGF-stimulated keratinocytes. *A* and *B*, immunohistochemical staining of phospho-ERK1/2 in wound sections at days 3 and 14. Phospho-ERK1/2 staining is higher in *Rhamm*$^{-/-}$ keratinocytes than WT at both day 3 and day 14. At day 14, phospho-ERK1/2 staining occurs throughout the *Rhamm*$^{-/-}$ epidermal layers but is restricted to the proliferating basal keratinocytes in WT mice. *B,* scatter plots of $n = 4$ slides with five replicate analyses for each slide. **, $p < 0.01$; ***, $p < 0.001$. *C*, cultured primary *Rhamm*$^{-/-}$ keratinocytes retain higher phospho-ERK1/2 levels than WT keratinocytes. Scatter plots of $n = 7$ replicates. *, $p < 0.05$. *D,* ERK1/2 activity is required for migration of both *Rhamm*$^{-/-}$ and WT primary keratinocytes, but *Rhamm*$^{-/-}$ keratinocyte migration is more strongly blocked by pathway inhibition using the MEK inhibitor PD98059 than WT comparators. Values are presented as percentage inhibition. Scatter plot of $n = 4$; ****, $p < 0.0001$.

intracellular functions therefore likely contributed to this aberrant effect of *Rhamm*-loss.

The processes of cell migration and proliferation are uncoupled in both fibroblasts and keratinocytes during fibrotic wound repair (6, 16, 75–77). For example, keratinocytes migrating under the clot to initiate wound re-covering do not proliferate, whereas keratinocytes in back of the wound edge proliferate to ensure the supply of migrating cells is sufficient to cover the wound (75). Non-proliferating fibroblasts contribute to wound closure not only by producing the ECM for keratinocytes to migrate on but also by differentiating into myofibroblasts to promote wound-site contraction (7, 75, 78). Deregulation of this temporal control is associated with abnormal skin repair.

Our results show that the key factors in the cell context–dependent regulation of migration by RHAMM are CD44 and MMP-9. Both keratinocytes and fibroblasts exhibit co-distribution as well as a functional interdependence of RHAMM, CD44, and MMP-9 activity for migration. However, RHAMM and CD44 suppress an EGFR–ERK1/2:MMP-9 pathway signaling required to promote keratinocyte migration. When this suppression is relieved, EGFR signaling is activated, and MMP-9 is expressed, which cleaves CD44 to promote migration. In contrast, dermal fibroblasts require RHAMM and CD44 to activate a PDGF receptor, TGFβ1, and/or a serum:ERK1/2 pathway that promotes MMP-9 expression, which is able to activate fibroblast motogens such as TGFβ1 (79) and which promotes focal adhesion formation (80) necessary for fibroblast migration. These results are summarized in the model shown in Fig. 16*A*.

CD44 is a hyaluronan and growth factor co-receptor that is subject to extensive alternative splicing. Its resulting biology is complex because although this receptor has most frequently been shown to promote cell adhesion and motility, for example (81, 82), an increasing number of reports are identifying context-dependent conditions where CD44 shedding or its genomic-loss is required for stimulation of motility. For example, blocking cleavage of CD44 prevents migration of glioma cells on HA substrates (83), and CD44 shedding or genetic-loss promotes migration of fibroblasts and other cells across small wound gaps (67). Conversely, fibroblasts require the surface display of CD44 for migrating across larger wound gaps that mimic excisional wounds (35). These few examples and the data presented in this study illustrate a mechanistic complexity and contextual dependence underlying regulation of cell migration during wound repair that is understudied and that needs to be addressed for the development of effective wound control.

Proteases, including ADAMS, and MMPs, such as MT1-MMP and MMP-9, cleave the ectodomains of a number of transmembrane proteins, including CD44 (84–86). MMP-9 proteolytic activity disrupts the cell–cell and cell–substratum adhesions that restrict keratinocyte and fibroblast migration (87–91),

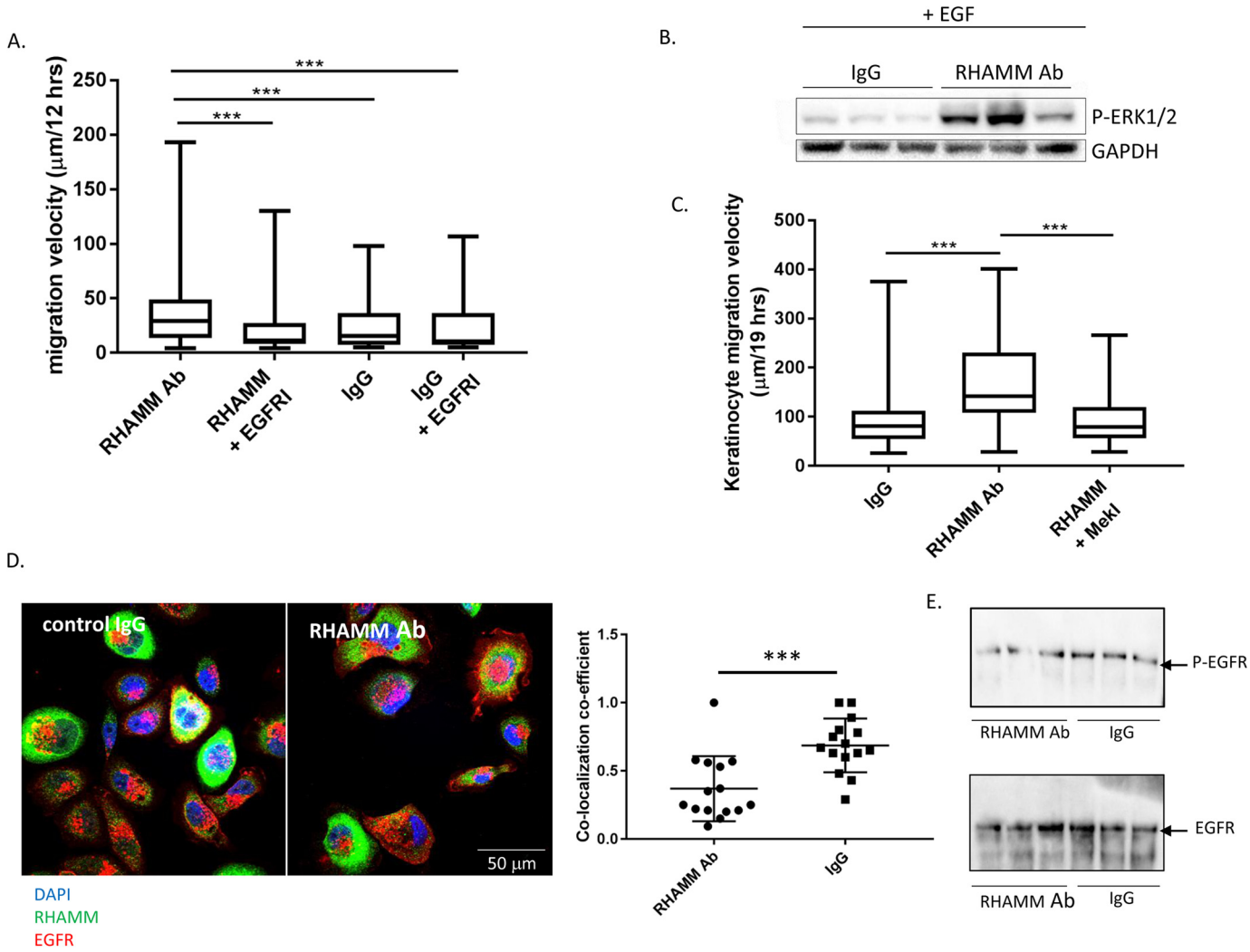

Figure 11. RHAMM regulates ERK1/2 motogenic signaling in EGF-stimulated keratinocytes. *A,* EGFR inhibition (*EGFRI*) blocks migration of HaCaT cells treated with RHAMM antibody but had no effect on IgG-treated cells. *Box* and *whisker plots* of $n = 35$ cells. *B,* RHAMM antibody stimulates ERK1/2 activation in HaCaT cells. Western blot analysis of HaCaT cells treated with RHAMM antibody or control IgG. *C,* addition of a MEK1,2 inhibitor (PD8059) to HaCaT keratinocytes blocks migration stimulated by the RHAMM antibody indicating that extracellular RHAMM regulates this pathway. *Box* and *whisker plot* of $n = 35$ cells. ***, $p < 0.001$. *D,* co-localization of RHAMM and EGFR is reduced by RHAMM antibodies. Scatter plots of $n = 15$ cells. *E,* EGFR activation is not affected by RHAMM antibodies. Western blot analysis is shown of active EGFR and total EGFR in HaCaT cells treated with RHAMM antibody or control IgG.

and MMP-9 loss delays re-epithelialization (92). This metalloproteinase can also promote motility by proteolytic-independent, hemopexin domain– dependent mechanisms (80, 93, 94). CD44 is a key MMP-9 – binding partner for both of these motogenic mechanisms. Our data suggest that *Rhamm*-loss is also a critical partner in these mechanisms since we show that blocking this protein promotes the proteolytic selectivity of MMP-9 for CD44, which results in increased keratinocyte migration.

In addition to its role in cell migration, RHAMM has also been reported to regulate cell proliferation. For example, RHAMM promotes progression of cultured cells through G_2M, and it contributes to mitotic spindle dynamics and orientation during development and disease (25, 26, 81, 95). However, our results support a dominant effect of RHAMM on migration rather than proliferation *per se,* as we were unable to observe a strong effect of *Rhamm*-loss on keratinocyte or fibroblast proliferation during excisional repair or in 2D culture. Keratinocyte migration and proliferation during cutaneous repair are uncoupled, which we also observed in WT excisional wounds of this study. *Rhamm*-loss appears to extend this period of uncoupling even after re-epithelialization of the wound has occurred. This subtle consequence of *Rhamm*-loss could alter stem cell re-population dynamics and contribute to the observed aberrant epidermal architecture. These results are consistent with a previous report documenting a role for RHAMM in coupling migration to the cell cycle (96).

In conclusion, a number of diseases (97, 98) result from aberrantly regulated keratinocyte migration, including skin disorders (*e.g.* ulcers), burns, diseases resulting from chronic inflammation, and the spread of keratinocyte cancers. The worldwide increase in patients with aberrant wound repair related to aging, diabetes, malnutrition, chemotherapy, and hereditary diseases provides an imperative for identifying the mechanisms of the healing steps in order to rationally manipulate and improve skin wound repair. Our results suggest that blocking RHAMM function could be used to accelerate keratinocyte migration in some of these skin disorders.

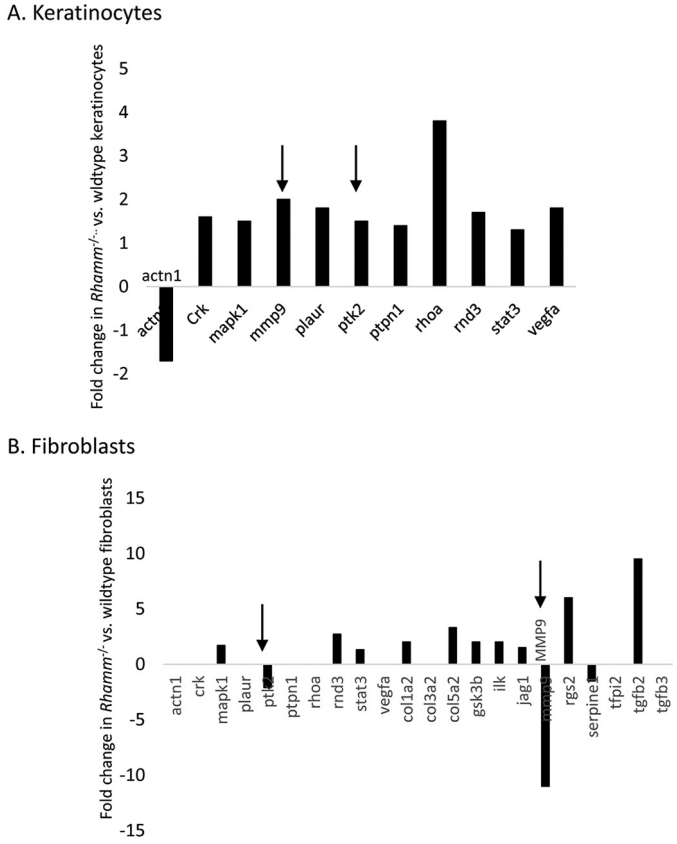

Figure 12. RHAMM differentially regulates MMP-9 mRNA expression in keratinocytes and fibroblasts. PCR (*A*) and Affymetrix (*B*) arrays were used to detect differences in expression of migration-related genes and were performed with mRNA isolated from primary keratinocytes and immortalized fibroblasts. *A*, RHAMM-loss increases *Mmp-9* and PTK2 mRNA expression in keratinocytes. *B,* RHAMM suppression decreases mRNA expression of these genes in fibroblasts. Values in *A* and *B* are mean and S.E. $n = 3$ replicates ($p < 0.05$).

Experimental procedures

Materials

Eagle's minimal essential media without Ca^{2+} (EMEM minus Ca^{2+}) were purchased from BioWhittaker/Lonza (Walkersville, MD). T-25 flasks were from Corning/Thermo Fisher Scientific (Nepean, Ontario, Canada). Human fibronectin was from BD Biosciences. Fetal bovine serum, penicillin/streptomycin, DMEM, 0.25% trypsin, PBS, and Dulbecco's PBS (D-PBS) were purchased from Wisent Bioproducts (St.-Bruno, Quebec, Canada). Chelex 100 was from Bio-Rad (Mississauga, Ontario, Canada). Insulin was from Invitrogen (Burlington, Ontario, Canada); L-glutamine was from GIBCO/Life Sciences (Burlington Ontario, Canada), and 2′-amino-3′ methoxyflavone (PD98059) and UO126 were purchased from Cell Signaling Technologies, (Danvers, MA). Hydrocortisone, 3,3′,5-triiodo-L-thyronine (T3), MMP-9 inhibitor I, and mouse EGF were purchased from Sigma-Aldrich (Oakville, Ontario, Canada). Cytoseal, anti-EGFR, and anti-CD44 antibodies were purchased from Thermo Fisher Scientific (Waltham, MA). Anti-pan-keratin, keratin 10, keratin 14, anti-MMP-9, anti-Ki67, anti-phospho-EGFR, anti-RHAMM antibodies, and the CD44 ELISA were purchased from AbCAM (Toronto, Ontario, Canada). Blocking EGFR antibodies were purchased from R&D Systems (Minneapolis, MN). Alexa 555- and Alexa 488–labeled secondary antibodies and ProLongGold antifade mounting medium were purchased from Invitrogen (Burlington, Ontario, Canada). Alexa 488–labeled anti-phospho-ERK1/2 antibody was purchased from Cell Signaling (Whitby, Ontario, Canada). Biotinylated secondary antibodies, streptavidin-HRP, and 3,3′-diaminobenzidine (DAB) Plus reagent were purchased from DAKO (Santa Clara, CA). Ambion TRIzol reagent, alamarBlue™ reagent, SuperScript VILO cDNA synthesis kit, SYBR Green mastermix, and primer were purchased from Thermo Fisher Scientific (Waltham, MA). RT^2 profiler PCR array and reverse transcriptase were purchased from Qiagen (Toronto, Ontario, Canada). Active MMP-9 was purchased from Enzo Life Sciences (Farmingdale, NY). Bolt 4–12% BisTris polyacrylamide gels and Bolt MES SDS running buffer were purchased from Invitrogen (Burlington, Ontario, Canada). Novex NuPAGE transfer buffer was purchased from Thermo Fisher Scientific, (Waltham, MA). Methanol was purchased from Sigma-Aldrich (Oakville, Ontario, Canada). 4× Laemmli Sample Buffer was purchased from Bio-Rad (Mississauga, Ontario, Canada). Luminate Forte Western HRP substrate and Immobilon-P transfer membrane were purchased from Millipore (Etobicoke, Ontario, Canada). The blocking RHAMM polyclonal antibody was prepared against mouse sequence VSIEKEKIDEKCETEK (99) (ProMab), and the antibody was affinity-purified using recombinant RHAMM affinity chromatography. The specificity of this antibody for RHAMM is verified using *Rhamm*$^{-/-}$ cells and cell lysates.

C57BL/6 mice were obtained from Charles River Laboratories; the preparation of C57BL/6 *Rhamm*$^{-/-}$ mice has previously been described and characterized (100), and deletion of exons 8–15 of the *Rhamm* gene is described in detail elsewhere (100). In brief, to delete exons 8–15 of the murine *Rhamm* gene, a construct was generated that consisted of the hypoxanthine-guanine phosphoribosyltransferase selection marker flanked by genomic *Rhamm* sequence upstream of exon 8 and downstream of exon 15. This construct was transfected by electroporation into Hprt-negative HM-1 mouse embryonic stem cells. Hprt-positive clones were isolated by selection in HAT medium. Clones with homologous recombination events were identified by Southern blotting analyses. *Rhamm*$^{+/-}$ ES cells were injected into C57BL/6 blastocysts that were implanted into pseudopregnant females. To generate *Rhamm*$^{+/-}$ mice, chimeric males were bred to C57BL/6 females. Breeding of *Rhamm*$^{+/-}$ males with *Rhamm*$^{+/-}$ females produced the expected ratio of WT, *Rhamm*$^{-/-}$, and *Rhamm*$^{+/-}$ offspring. WT and *Rhamm*$^{-/-}$ mice, which were maintained as homozygotes on a C57BL/6 background, were cared for in keeping with the Guide to the Care and use of Experimental Animals from the Canadian Council on Animal Care, and our use of mice was reviewed and approved (protocol 2009-060) by the Animal Care Committees at the London Regional Health Centre and University of Western Ontario. Food and water access were *ad libitum*. For breeding, adult C57Bl/6 males were housed with two C57Bl/6 females until pregnancy was obvious, at which time pregnant females were housed individually. For keratinocyte isolation, newborn pups were removed and euthanized by 30 min of CO_2 inhalation.

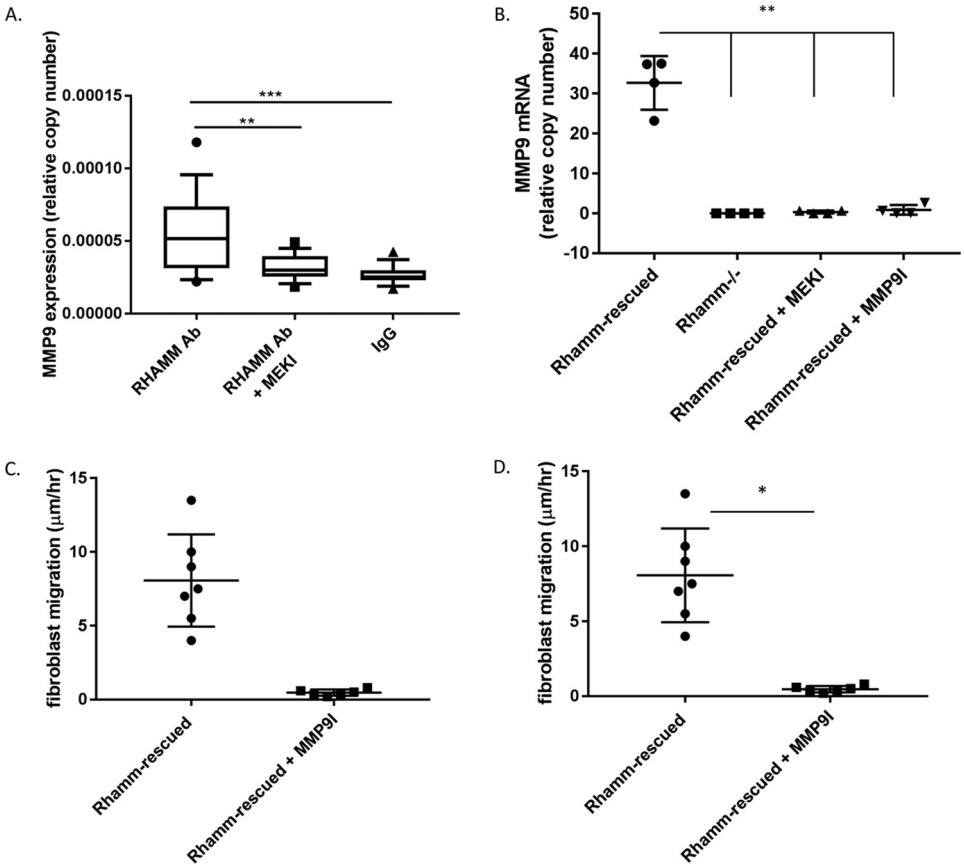

Figure 13. MMP-9 expression is regulated by ERK1/2 in keratinocytes and fibroblasts and is required for migration of both cell types. *A,* RHAMM-blocking antibody significantly increases the expression of *MMP-9* mRNA in HaCaT keratinocytes as detected by qRT-PCR using *GAPDH* as a loading control. Expression is reduced by inhibiting ERK1/2 activity with the MEK inhibitor PD98059. *Box* and *whisker plot* of $n = 9$ replicates. *B*, *Rhamm*$^{-/-}$ fibroblasts express little *MMP-9* mRNA and expression is increased by *Rhamm*-rescue. The increased in MMP-9 expression stimulated by *Rhamm*-rescue is blocked by inhibiting ERK1/2 activity using PD98059. Scatter plot of $n = 4$ replicates. *C*, keratinocyte migration stimulated by the RHAMM antibody is blocked by inhibiting MMP-9 activity. *Box* and *whisker plot* of $n = 25$. *D,* fibroblast migration stimulated by *Rhamm*-rescued is blocked by inhibiting MMP-9 activity. Values are the mean and S.E. $n = 60$ cells/condition. *, $p < 0.05$; **, $p < 0.01$; ***, $p < 0.001$

Methods

Genotyping—Frozen tail samples were digested overnight at 55 °C in 350 μl of lysis buffer containing 50 mM Tris, 0.1 M EDTA, pH 8, 1% SDS, 100 mM NaCl, 800 μg/ml proteinase K. Samples were continuously mixed at 800 rpm during the digest. Digested samples were centrifuged at 15,500 × *g* for 10 min to remove debris. The supernatant was retrieved and mixed with 500 μl of isopropyl alcohol. Samples were centrifuged again at 15,500 × *g* for 15 min to pellet the DNA. The supernatant was decanted, and the DNA pellet was washed twice with 500 μl ice cold 70% ETOH, dried at room temperature for several hrs and the pellet was dissolved in 100 μl ddH_2O. DNA concentration was measured using a NANODROP instrument and adjusted to a concentration of 50 ng/μl.

For primer sequencing, the following sequences were used: *Rhamm* knockout FW PR3, CCT CAT GGA CTG ATT ATG, and *Rhamm* knockout RV PR3, CCA ACA AAG TCT GGC CTG; WT-3, CCT CAA GAG ACT GCT TAA GAC; and WT-5, GTT TCA ATA GAG AAA GAA AAG ATC.

For PCR mixtures, the following were used: forward primer (0.5 μM) 0.125 μl, reverse primer (0.5 μM) 0.125 μl; ultrapure ddH_2O 10.25 μl ; GC mix enhancer 1.00 μl; DNA 1.00 μl; AmpliTaq 360 mastermix 12.5 μl.

The following PCR conditions were used: 1. incubate at 94 °C for 15 min; 2. incubate at 94 °C for 30 s; incubate at 50 °C for 1 min (WT allele) or 55 °C for 1 min (Rhamm knock out allele); incubate at 72 °C for 1 min. Return to step 2 for 39 more times. Incubate at 72 °C for 10 min and hold at 4 °C. Add 2 μl of 6× DNA loading buffer to 10 μl of PCR sample and run sample on a 1% agarose gel.

Excisional wounding—All animal experiments followed policies and guidelines established by the Canadian Council for Animal Care and were previously approved by the Animal Use Committee of Western University (protocol no. 2009-060). Excisional wounds were placed as described previously (35). In brief, 8–12-month-old female *Rhamm*$^{-/-}$ and WT mice were anesthetized using isoflurane inhalation. Dorsal hair was removed using an electric razor. Using a metal punch with a 4-mm diameter, one full-thickness punch biopsy was taken from the middle of the dorsum, resulting in two full-thickness skin wounds. Using an 8-mm metal punch, the wound area was harvested at different times after wounding. Wound samples were fixed in 4% paraformaldehyde/phosphate buffered saline (PBS) at pH 7.4, and paraffin was processed for histology tissue sections.

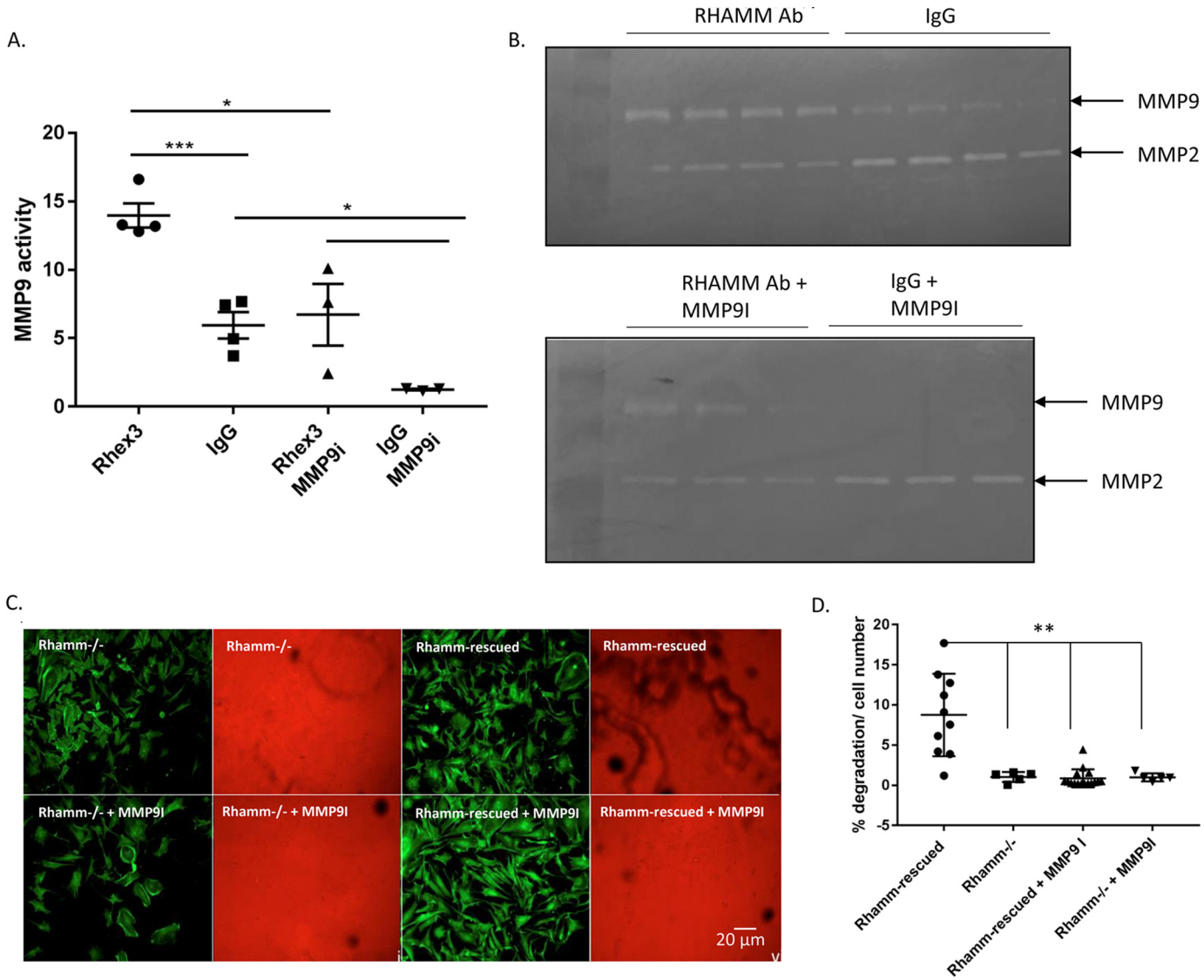

Figure 14. RHAMM regulates MMP-9 activity. *A* and *B*, scratch wounds of HaCaT keratinocyte cultures were treated with either RHAMM antibodies or control IgG. MMP-9 activity in conditioned medium was analyzed by zymogram gels. RHAMM antibodies increased MMP-9 activity. MMP-9 activity was inhibited by an MMP-9 inhibitor, demonstrating its specificity. *A,* scatter plot of $n = 3–4$. *, $p < 0.05$; ***, $p < 0.001$. *B,* zymogram images. *C* and *D*, MMP-9 activity in fibroblasts is rescued by RHAMM expression. *C,* images of collagen degradation. *D,* scatter plot of $n = 10$ cells. **, $p < 0.01$.

Immunohistochemistry—Paraffin-processed tissue sections were obtained as described previously (35). In brief, sections were de-paraffinized by passage through xylene and an ethanol series. Antigen retrieval was performed by boiling slides in 0.01 M sodium citrate, pH 6, for 20 min using a microwave. Endogenous peroxidase was blocked by incubating slides for 10 min in 3% H_2O_2/PBS at room temperature. Nonspecific antibody binding was blocked by incubating slides in 3% BSA/PBS for 1 h at room temperature. Primary antibodies were diluted 1:250 in 1% BSA/PBS and added to the slides. IgG was used as negative control. Slides were incubated overnight with antibodies (pan-keratin, p-ERK1/2) at 4 °C in a humidified chamber at dilutions recommended by the manufacturer. Slides were then washed in PBS and incubated with a biotinylated secondary antibody (1:500 in 1% BSA/PBS) for 1 h at room temperature. Slides were washed to remove unbound secondary antibody, and washed slides were incubated with streptavidin-HRP (1:500 in PBS) for 1 h at room temperature to visualize bound streptavidin secondary antibodies. Slides were washed to remove unbound streptavidin-HRP, which was then visualized using DAB Plus according to the manufacturer's instructions. Slides were counterstained with hematoxylin, washed, passed through an increasing ethanol series followed by xylene, and mounted using Cytoseal 60.

Image analysis of immunohistochemistry—Slides were scanned using an Aperio Scan Scope or photographed using an AX70 Provis Olympus microscope equipped with air objectives (×4, NA 0.16; ×20, NA 0.7; Olympus, Tokyo, Japan) and a color camera (Cooke SensiCam CCD imaging; PCO-TECH, Romulus, MI) controlled by Image-Pro Plus 4.5.1.2.9 (Media Cybernetics, Rockville, MD) software. Images were saved as tiff files which were then analyzed by ImageJ software (RRID: SCR_003070). Color deconvolution was performed using the DAB/hematoxylin setting of the color deconvolution plugin. Using the threshold function and by comparing images of antibody *versus* control nonimmune IgG, brown pixels were

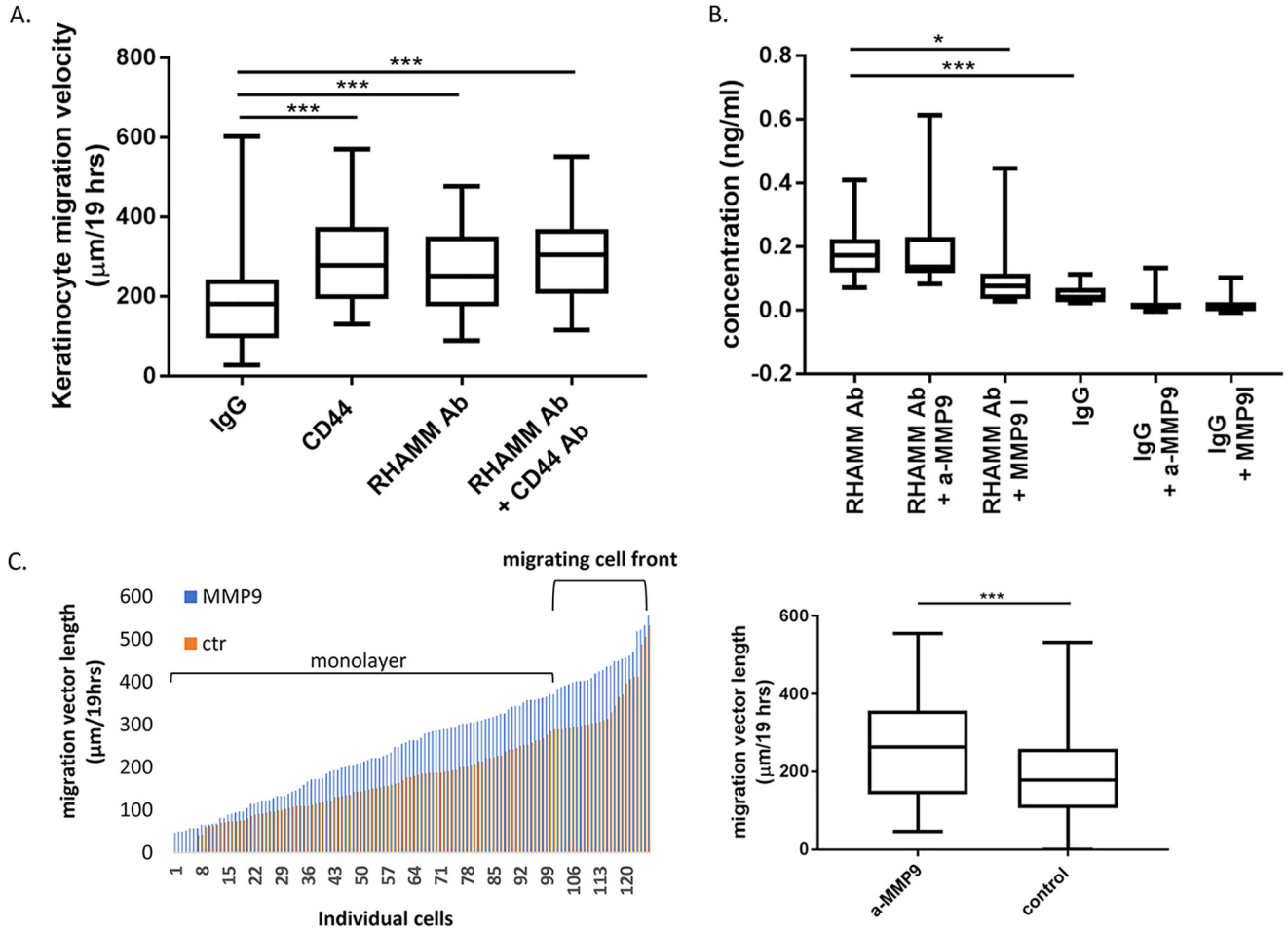

Figure 15. Loss of CD44 promotes keratinocyte migration and RHAMM regulates CD44 shedding. *A,* CD44 function-blocking antibody increases HaCaT motility to a similar extent as the RHAMM antibody. Addition of both antibodies together does not further increase motility predicting that CD44 and RHAMM are acting on the same motogenic pathway. *Box* and *whisker plots* of $n = 65$ cells/condition. *B,* RHAMM antibody increases CD44 shedding, which requires MMP-9 activity. Shedding was quantified using a CD44 ELISA that detects all CD44 isoforms. *Box* and *whisker plots* of $n = 6$ replicates. *a-MMP-9,* activated recombinant MMP-9 protein; *MMP-9I,* MMP-9 inhibitor. *C,* a-MMP-9 stimulates HaCaT keratinocytes migration, which was quantified with a scratch-wound assay. *Left panel* shows migration vectors of individual cells, and *right panel* shows the averaged motility of HaCaT keratinocytes exposed to active MMP-9 protein or buffer alone. Values are the mean and S.E. $n = 120$. *, $p < 0.05$; ***, $p < 0.001$.

selected. The number of selected pixels in a constant region of interest was quantified using the analysis function.

Primary keratinocyte culture—Primary keratinocytes from 1- to 2-day-old *Rhamm*$^{-/-}$ or WT mouse pups were isolated (101, 102) and cultured on fibronectin-coated (50 μg/ml) T-25 flasks in Keratinocyte Growth Media (EMEM minus Ca^{2+}, 10% FBS (Chelex-treated to remove Ca^{2+})), insulin (5 μg/ml), hydrocortisone (74 ng/ml), T3 (6.7 ng/ml), penicillin (100 units/ml), streptomycin (100 μg/ml), L-glutamine 29.2 mg/ml, and EGF (5 ng/ml). The keratinocytes were incubated for 24 h at 37 °C with 5% CO_2. The flasks were then rinsed twice with fresh media before experimental analyses.

Fibroblast cultures—Primary WT and *Rhamm*$^{-/-}$ dermal fibroblasts were isolated from explanted skin. Immortalized *Rhamm*$^{-/-}$ fibroblasts were obtained as described previously and rescued by transfection with a full-length mouse *Rhamm* cDNA. Cells were plated onto fibronectin-coated culture flasks (Falcon) for 12 h and then placed on a heated stage (Tokai Hit/Nikon, Mississauga, Ontario, Canada) at 37 °C, and the displacement of cells was recorded at 5-min intervals for 12 h by video microscopy using a Nikon Eclipse TE300 microscope (Mississauga, Ontario, Canada) with NSI Elements AR software (Nikon), and a Hewlett Packard computer (Mississauga, Ontario, Canada).

HaCaT keratinocyte cell line—This human keratinocyte cell line (HaCaT) was a kind gift from Dr. Trevor Shepherd (London Regional Cancer Program). Cells were grown in growth medium (DMEM with 10% FBS and 1× antibiotic/antimycotic) at 37 °C at 5% CO_2. Cells were passaged at 80% confluence by incubating the monolayer in 10 ml of D-PBS containing 0.2 mM EDTA for 15 min at 37 °C. The D-PBS/EDTA solution was removed, and the monolayers were then incubated with 2 ml of 0.25% trypsin for 10 min, which was stopped by adding fresh DMEM + 10% FBS. Dispersed cells were recovered by centrifugation (100 × *g*) and subcultured at a 1:5 dilution into DMEM + 10% FBS.

Cell motility of primary keratinocytes, HaCaT keratinocytes, and fibroblasts—Cells were washed with DMEM, and fresh growth medium was added to the flasks. RHAMM antibody (1:50 dilution) or nonimmune IgG was added to the media. Inhibitors PD98059 (50 μM) and UO126 (50 μM) were added to the media. Control media contained the same concentration of

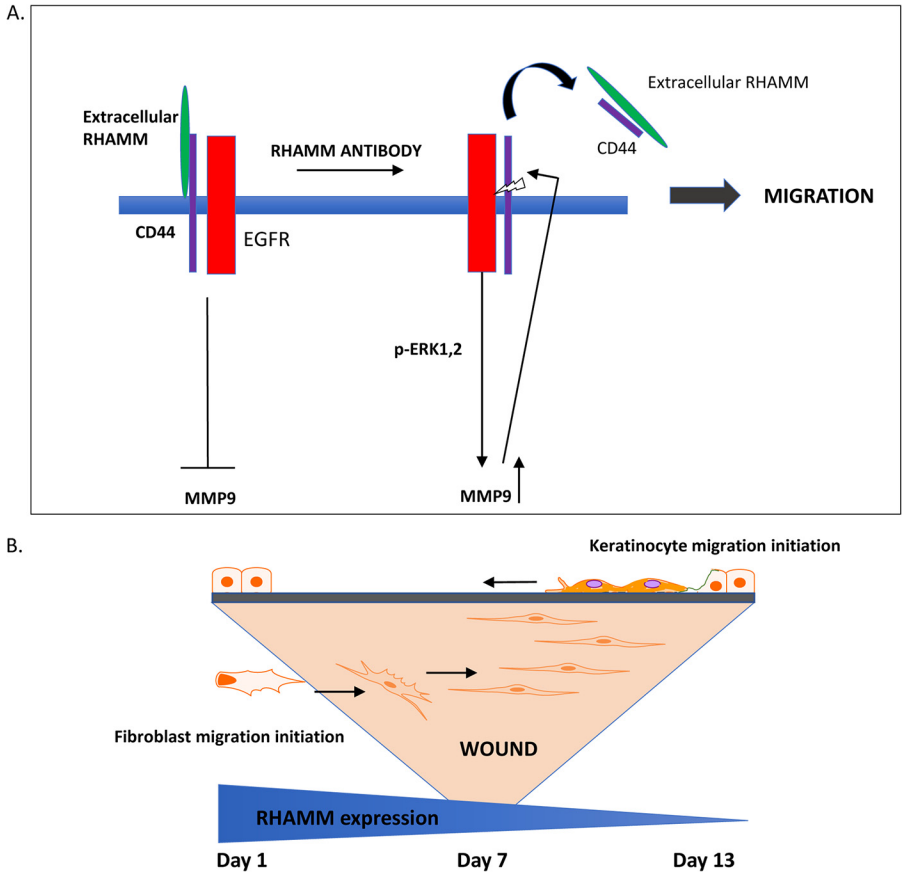

Figure 16. Models for RHAMM-regulated motogenic signaling in keratinocytes and temporal-spatial coordination of keratinocyte and fibroblast migration in excisional wounds. *A,* signaling model for regulation of keratinocyte migration by RHAMM. RHAMM/CD44 interactions block EGFR-regulated ERK1/2 activity and downstream expression of the motogenic target gene, *MMP-9*. Blocking extracellular RHAMM function releases the pathway and stimulates the expression and release of MMP-9, which promotes CD44 shedding, resulting in increased keratinocyte migration. *B,* RHAMM expression is ubiquitous in wounds by 24 h after excisional injury and then decreases over time. Maximal expression corresponds to influx of innate immune cells and initiation of fibroblast migration to form granulation tissue. As RHAMM protein levels decrease, keratinocyte migration is initiated. Aberrant RHAMM expression alters the timing of keratinocyte and fibroblast migration resulting in altered rate of wound closure and dysregulated differentiation within the wound site.

DMSO (0.1%) as the inhibitor-containing media, and cells were incubated for 1 h at 37 °C with 5% CO_2 prior to filming. Sealed flask(s) were placed on a heated stage (Tokai Hit/Nikon, Mississauga, Ontario, Canada) at 37 °C, and the displacement of cells was recorded at 5-min intervals for 12 h by video microscopy using a Nikon Eclipse TE300 microscope (Mississauga, Ontario, Canada) with NSI Elements AR software (Nikon), and a Hewlett Packard computer (Mississauga, Ontario, Canada). The NSI Elements AR analysis program (Nikon) was used to track the path length of each migrating cell and to calculate the total distance traveled by each cell at the corresponding time, which was used to calculate the migration velocity of each cell. Individual migration rates as well as the recorded population average were calculated and graphed on GraphPad software. Directional persistence was defined as the total distance from origin (in micrometers) divided by the net path length (in micrometers) (103).

HaCaT scratch-wound assay—HaCaT cells were plated onto fibronectin-coated IBIDI 8-well chambers using a cell density that achieved confluence after overnight incubation in growth medium. The next day, the monolayer was scratch-wounded with a 1000-μl (blue) pipette tip. Detached cells were removed by gentle washing, and injured monolayers were incubated with blocking RHAMM antibody or control IgG in low-calcium keratinocyte medium containing 10% calcium-free FBS overnight ± 10 nM MMP-9 inhibitor I, 10 ng/ml active MMP-9 recombinant protein, or 1:100 blocking CD44 antibody or blocking EGFR antibody (10 μM). DMSO was included in controls where relevant. Cell migration was analyzed by time-lapse video microscopy with images taken at 5-min intervals for 24 h using the above Nikon microscope equipped with NSI Elements AR software. The NSI Elements AR analysis program was then used to measure the distance between the cell front at time 0 and individual cells after 12 h. Results were copied to EXCEL and then sorted from lowest to highest value and displayed in a bar graph.

Immunofluorescent staining and co-localization analysis—Scratch-wounded, subconfluent HaCaT keratinocytes were exposed to the blocking RHAMM antibody or nonimmune IgG as above for 24 h and then fixed in 4% paraformaldehyde/PBS, pH 7.5, for 10 min at room temperature. Fixed cells were washed to remove fixative and then incubated for 10 min at room temperature with 0.01% Triton X-100/PBS. Nonspecific antibody-binding sites were blocked with 3% BSA/PBS for 1 h. Coverslips were then incubated with primary antibodies (EGFR, IQGAP1 1:500; RHAMM 1:250; CD44 1:250; Ki67 1:200, Alexa 488 ERK 1:100 or nonimmune IgG) overnight at 4 °C, washed, and then incubated with fluorescent secondary

antibodies (1:200) for 1 h at room temperature, with the exception of the fluorescently-labeled p-ERK antibody, which was immediately mounted in DAPI-containing ProLong Gold antifade mounting reagent. Coverslips were washed in PBS and then mounted with DAPI-containing ProLong Gold anti-fade mounting reagent as above. Cells were imaged using an IX81 Olympus confocal microscope equipped with FV10-ASW 4.2 software, and images were saved as tiff files. Co-localization and fluorescent intensity were quantified using ImageJ. Fluorescent channels were separated (Image-Color-Split Channels), and the co-localization of red and green channel was determined using the co-localization plugin (Analyze-Co-localization-Co-localization Threshold). Fluorescence intensity was quantified using the "Measure" function.

The protocol for immunofluorescent staining of paraffin-embedded sections was similar to immunohistochemistry described above, with the endogenous peroxidase quenching step omitted. Nonspecific antibody binding was blocked using 3% BSA/PBS at room temperature for 1 h, and intermediate washing steps were performed using PBS. Primary antibodies (RHAMM, keratin 10, keratin 14, and PAR) were added to slides at dilutions recommended by the manufacturer, with nonimmune IgG used as the negative control. All slides were incubated overnight in humidifying chambers at 4 °C. Following three washes in PBS, fluorescent secondary antibody (Alexa 488, 1:100) was added to slides incubated at room temperature for 2 h and then washed in PBS. All slides were mounted with DAPI-containing ProLong Gold anti-fade mounting reagents and imaged using an IX81 Olympus confocal microscope. Quantification of staining was performed with ImageJ.

Cell proliferation analysis—Subconfluent HaCaT cell cultures were stained with Ki67 antibody as described above. Cell proliferation of HaCaT keratinocytes and dermal fibroblasts were quantified by counting Ki67-positive and -negative nuclei and calculating the percentage of Ki67-positive nuclei.

CD44 ELISA—Sufficient HaCaT cells were seeded onto fibronectin-coated 6-well plates to generate confluent monolayers after 24 h. Four scratch wounds/well were placed using a 1000-μl blue pipette tip, and cultures were gently washed with keratinocyte growth medium to remove detached cells. Keratinocyte growth medium ± active MMP-9 recombinant protein (10 ng/ml), blocking RHAMM Ab, and/or nonimmune IgG were then added for 20 h at 37 °C, and culture medium was collected and centrifuged at 1000 × *g* for 4 min. Supernatant was added to the CD44 ELISA plate undiluted (200 μl/well), and the plate was incubated overnight at 4 °C. Detection of CD44 was performed as described in the manufacturer's instructions.

RT-PCR analysis—Total RNA was isolated from cultures of migrating cells using TRIzol reagent (1 ml/plate) according to the manufacturer's instructions. Cells were scraped off using rubber cell scrapers, and detached cells were mixed with 200 μl of chloroform and centrifuged at 15,500 × *g* for 10 min at 4 °C. The top phase was pipetted and mixed with 500 μl of isopropyl alcohol to precipitate RNA. Samples were stored at −20 °C overnight and then centrifuged at 15,500 × *g* at 4 °C for 30 min. Isopropyl alcohol was removed, and the RNA pellet was washed with 70% ice-cold ethanol, and centrifuged at 15,500 × *g* at 4 °C for 15 min. Ethanol was removed from the precipitated RNA pellet, which was dried at room temperature, dissolved in 100 μl of ultrapure ddH_2O, and measured using a NANODROP instrument. 2 μg of RNA was used to synthesize cDNA with the RT^2 Profiler reverse transcription kit used according to the manufacturer's instructions. RT^2 Profiler PCR arrays were used and analyzed following manufacturer's instructions.

MMP-9 qRT-PCR—Subconfluent HaCaT cells were treated with RHAMM antibody or IgG as described above. RNA was isolated using TRIzol reagent and following the manufacturer's instructions. RNA concentration was determined using a NANODROP instrument. 2 μg of RNA was used to synthesize cDNA with SuperScript VILO cDNA synthesis kit and following the manufacturer's instructions. cDNA was diluted 1:10 with ddH_2O, and 2 μl of diluted cDNA was used per qPCR. SYBR Green mastermix, *MMP-9*–specific primers, and 2 μl of diluted cDNA were used for each qRT-PCR. *GAPDH* was used as a housekeeping gene. Fold-expression was calculated using the Δ*CT* method. Mouse fibroblast *MMP-9* mRNA expression was performed as described previously (93).

For primer sequencing, the following sequences were used: *MMP-9* FW TGTACCGCTATGGTTACACTCG and *MMP-9* RV GGCAGGGACAGTTGCTTCT; *GAPDH* FW GGAGCGAGATCCCTCCAAAAT and *GAPDH* RV GGCTGTTGTCATACTTCTCATGG.

PCR conditions: 1. incubate at 94 °C for 10 min; 2. incubate at 94 °C for 30 s; incubate at 55 °C for 45 s; and incubate at 72 °C for 45 s. Return to step 2 for 39 more times. Incubate at 72 °C for 10 min.

Western blotting assays—Subconfluent HaCaT cell cultures were treated with RHAMM antibody or IgG as described above. Cells were washed once with cold PBS and then lysed in RIPA buffer containing proteinase and phosphatase inhibitors. Protein concentration was determined using BCA protein assay kit following the manufacturer's instructions. Laemmli sample buffer was added to the lysate, and samples were heated to 95 °C for 5 min. 30 μg of protein per sample were loaded onto Bolt 4–12% polyacrylamide gels. Following electrophoresis, gels were transferred on Immobilon-P transfer membrane using NuPAGE transfer buffer containing 10% methanol. Membranes were blocked with TBS-T (TBS plus 0.25% Tween 20) containing 5% skim milk overnight at 4 °C. Primary antibodies (RHAMM, p-EGFR, and p-ERK1/2, AbCAM) were diluted 1:500 to 1:1000 in TBS-T containing 1% milk. Membranes were incubated with primary antibodies for 2 h at room temperature, washed with TBS-T three times for 10 min, then incubated with 1:2000 diluted secondary HRP-coupled antibody for 1 h at room temperature, and washed with TBS-T three times for 10 min. Membranes were incubated with HRP substrate and imaged using Image Lab software (Bio-Rad). Protein bands were quantified using Image Lab software.

Zymograms—HaCaT cells were cultured on fibronectin-coated 6-cm cell culture plates using DMEM plus 10% FBS and antibiotics/antimycotics. Confluent cultures were scratch-wounded using a blue pipette tip. Cultures were washed once with serum-free Keratinocyte Growth Medium containing EGF. Cells were cultured overnight in serum-free Keratinocyte Growth Medium plus EGF, containing either RHAMM Ab or

IgG. Conditioned medium was mixed with 2× Tris-glycine SDS Sample buffer (Novex/Thermo Fisher Scientific), and 30 ml/well were loaded onto a zymogram gel containing gelatin (Novex/Thermo Fisher Scientific). 1× Tris-glycine SDS running buffer (Novex/Thermo Fisher Scientific) was used during gel electrophoresis. Following gel electrophoresis, gels were incubated two times for 30 min at room temperature in 1× zymogram Renaturation buffer (Novex/Thermo Fisher Scientific). Gels were then incubated for 30 min at room temperature in 1× Zymogram Developing buffer (Novex/Thermo Fisher Scientific) followed by 36 h of incubation at 37 °C in 1× Zymogram Developing buffer. Where indicated, MMP-9 inhibitor was added to the Developing buffer. Zymograms were stained with Coomassie Blue (2.5 of Coomassie Brilliant Blue in 450 ml of methanol, 100 ml of acetic acid, 450 ml of H_2O) for 2 h at room temperature followed by de-staining in de-staining solution (450 ml of methanol, 100 ml of acetic acid, 450 ml of H_2O). Stained gels were imaged with a digital camera. Degraded areas were quantified using ImageJ software.

For cell zymograms, fibroblasts were plated onto RITC-fibronectin (Cytoskeleton)-coated tissue coverslips and grown for 12 h. Cultures were fixed in 3% paraformaldehyde, washed, and mounted in ProLong Gold anti-fade mounting reagents and imaged using an IX81 Olympus confocal microscope. Areas cleared of RITC-fibronectin were quantified using ImageJ.

Statistical analyses—A two-way Student's *t* test was used to determine statistical significance between two experimental groups. A p value of <0.05 was considered to be statistically significant.

Author contributions—C. T., M. L., K. C., P. T., K. A., J. M., L. M., J. B. M., V. L. M., and E. A. T. conceptualization; C. T., M. L., K. C., P. T., K. A., J. M., L M., V. L. M., and E. A. T. data curation; C. T., M. L., P. T., and J. B. M. writing-review and editing; V. L. M. and E. A. T. supervision; V. L. M. and E. A. T. writing-original draft; E. A. T. funding acquisition.

References

1. Lindley, L. E., Stojadinovic, O., Pastar, I., and Tomic-Canic, M. (2016) Biology and biomarkers for wound healing. *Plast. Reconstr. Surg.* **138,** 18S–28S CrossRef Medline
2. Fang, R. C., and Mustoe, T. A. (2008) Animal models of wound healing: utility in transgenic mice. *J. Biomater. Sci. Polym. Ed.* **19,** 989–1005 CrossRef Medline
3. Greaves, N. S., Ashcroft, K. J., Baguneid, M., and Bayat, A. (2013) Current understanding of molecular and cellular mechanisms in fibroplasia and angiogenesis during acute wound healing. *J. Dermatol. Sci.* **72,** 206–217 CrossRef Medline
4. Bielefeld, K. A., Amini-Nik, S., and Alman, B. A. (2013) Cutaneous wound healing: recruiting developmental pathways for regeneration. *Cell. Mol. Life Sci.* **70,** 2059–2081 CrossRef Medline
5. Ud-Din, S., and Bayat, A. (2017) Non-animal models of wound healing in cutaneous repair: *in silico*, *in vitro*, *ex vivo*, and *in vivo* models of wounds and scars in human skin. *Wound Repair Regen.* **25,** 164–176 CrossRef Medline
6. Usui, M. L., Mansbridge, J. N., Carter, W. G., Fujita, M., and Olerud, J. E. (2008) Keratinocyte migration, proliferation, and differentiation in chronic ulcers from patients with diabetes and normal wounds. *J. Histochem. Cytochem.* **56,** 687–696 CrossRef Medline
7. Ding, J., and Tredget, E. E. (2015) The role of chemokines in fibrotic wound healing. *Adv. Wound Care* **4,** 673–686 CrossRef Medline
8. DiPersio, C. M., Zheng, R., Kenney, J., and Van De Water, L. (2016) Integrin-mediated regulation of epidermal wound functions. *Cell Tissue Res.* **365,** 467–482 CrossRef Medline
9. Finnson, K. W., Arany, P. R., and Philip, A. (2013) Transforming growth factor β signaling in cutaneous wound healing: lessons learned from animal studies. *Adv. Wound Care* **2,** 225–237 CrossRef Medline
10. Guo, S., and Dipietro, L. A. (2010) Factors affecting wound healing. *J. Dent. Res.* **89,** 219–229 CrossRef Medline
11. Xue, M., and Jackson, C. J. (2015) Extracellular matrix reorganization during wound healing and its impact on abnormal scarring. *Adv. Wound Care* **4,** 119–136 CrossRef Medline
12. Olczyk, P., Mencner, Ł., and Komosinska-Vassev, K. (2014) The role of the extracellular matrix components in cutaneous wound healing. *Biomed. Res. Int.* **2014,** 747584 **CrossRef Medline**
13. Chen, J., Chen, Y., Chen, Y., Yang, Z., You, B., Ruan, Y. C., and Peng, Y. (2016) Epidermal CFTR suppresses MAPK/NF-κB to promote cutaneous wound healing. *Cell. Physiol. Biochem.* **39,** 2262–2274 CrossRef Medline
14. Makino, K., Jinnin, M., Aoi, J., Kajihara, I., Makino, T., Fukushima, S., Sakai, K., Nakayama, K., Emoto, N., Yanagisawa, M., and Ihn, H. (2014) Knockout of endothelial cell-derived endothelin-1 attenuates skin fibrosis but accelerates cutaneous wound healing. *PLOS One* **9,** e97972 CrossRef Medline
15. Werner, S., Krieg, T., and Smola, H. (2007) Keratinocyte-fibroblast interactions in wound healing. *J. Invest. Dermatol.* **127,** 998–1008 CrossRef Medline
16. Shaterian, A., Kao, S., Chen, L., DiPietro, L. A., Coimbra, R., Eliceiri, B. P., and Baird, A. (2013) The candidate tumor suppressor gene Ecrg4 as a wound terminating factor in cutaneous injury. *Arch. Dermatol. Res.* **305,** 141–149 CrossRef Medline
17. Bradshaw, M., Clemons, T. D., Ho, D., Gutiérrez, L., Lázaro, F. J., House, M. J., St Pierre, T. G., Fear, M. W., Wood, F. M., and Iyer, K. S. (2015) Manipulating directional cell motility using intracellular superparamagnetic nanoparticles. *Nanoscale* **7,** 4884–4889 CrossRef Medline
18. de Campos, P. S., Matte, B. F., Diel, L. F., Jesus, L. H., Bernardi, L., Alves, A. M., Rados, P. V., and Lamers, M. L. (2017) Low doses of *Curcuma longa* modulates cell migration and cell–cell adhesion. *Phytother. Res.* **31,** 1433–1440 CrossRef Medline
19. Lee, D. E., Ayoub, N., and Agrawal, D. K. (2016) Mesenchymal stem cells and cutaneous wound healing: novel methods to increase cell delivery and therapeutic efficacy. *Stem Cell Res. Ther.* **7,** 37 CrossRef Medline
20. Kenny, F. N., and Connelly, J. T. (2015) Integrin-mediated adhesion and mechano-sensing in cutaneous wound healing. *Cell Tissue Res.* **360,** 571–582 CrossRef Medline
21. Martins-Green, M. (2013) The yin and yang of integrin function in re-epithelialization during wound healing. *Adv. Wound Care* **2,** 75–80 CrossRef Medline
22. Simone, T. M., Higgins, C. E., Czekay, R. P., Law, B. K., Higgins, S. P., Archambeault, J., Kutz, S. M., and Higgins, P. J. (2014) SERPINE1: a molecular switch in the proliferation-migration dichotomy in wound-"activated" Keratinocytes. *Adv. Wound Care* **3,** 281–290 CrossRef Medline
23. Volk, S. W., Iqbal, S. A., and Bayat, A. (2013) Interactions of the extracellular matrix and progenitor cells in cutaneous wound healing. *Adv. Wound Care* **2,** 261–272 CrossRef Medline
24. Peplow, P. V., and Chatterjee, M. P. (2013) A review of the influence of growth factors and cytokines in *in vitro* human keratinocyte migration. *Cytokine* **62,** 1–21 CrossRef Medline
25. Hauser-Kawaguchi, A., Luyt, L. G., and Turley, E. (2018) Design of peptide mimetics to block pro-inflammatory functions of HA fragments. *Matrix Biol.* **79,** 346–356 CrossRef Medline
26. Misra, S., Hascall, V. C., Markwald, R. R., and Ghatak, S. (2015) Interactions between hyaluronan and its receptors (CD44, RHAMM) regulate the activities of inflammation and cancer. *Front. Immunol.* **6,** 201 CrossRef Medline

27. Joy, R. A., Vikkath, N., and Ariyannur, P. S. (2018) Metabolism and mechanisms of action of hyaluronan in human biology. *Drug Metab. Pers. Ther.* **33,** 15–32 CrossRef Medline
28. Tavianatou, A. G., Caon, I., Franchi, M., Piperigkou, Z., Galesso, D., and Karamanos, N. K. (2019) Hyaluronan: molecular size-dependent signaling and biological functions in inflammation and cancer. *FEBS J.* **15,** 2883–2908 CrossRef Medline
29. Meier, C., Spitschak, A., Abshagen, K., Gupta, S., Mor, J. M., Wolkenhauer, O., Haier, J., Vollmar, B., Alla, V., and Pützer, B. M. (2014) Association of RHAMM with E2F1 promotes tumour cell extravasation by transcriptional up-regulation of fibronectin. *J. Pathol.* **234,** 351–364 CrossRef Medline
30. Maxwell, C. A., McCarthy, J., and Turley, E. (2008) Cell-surface and mitotic-spindle RHAMM: moonlighting or dual oncogenic functions? *J. Cell Sci.* **121,** 925–932 CrossRef Medline
31. Chen, H., Mohan, P., Jiang, J., Nemirovsky, O., He, D., Fleisch, M. C., Niederacher, D., Pilarski, L. M., Lim, C. J., and Maxwell, C. A. (2014) Spatial regulation of Aurora A activity during mitotic spindle assembly requires RHAMM to correctly localize TPX2. *Cell Cycle* **13,** 2248–2261 CrossRef Medline
32. Liu, M., Tolg, C., and Turley, E. (2019) Dissecting the dual nature of hyaluronan in the tumor microenvironment. *Front. Immunol.* **10,** 947 CrossRef Medline
33. Cui, Z., Liao, J., Cheong, N., Longoria, C., Cao, G., DeLisser, H. M., and Savani, R. C. (2018) The receptor for hyaluronan-mediated motility (CD168) promotes inflammation and fibrosis after acute lung injury. *Matrix Biol.* **79,** 255–271 CrossRef Medline
34. Wu, J., Qu, Y., Zhang, Y. P., Deng, J. X., and Yu, Q. H. (2018) RHAMM induces progression of rheumatoid arthritis by enhancing the functions of fibroblast-like synoviocytes. *BMC Musculoskelet. Disord.* **19,** 455 CrossRef Medline
35. Tolg, C., Hamilton, S. R., Nakrieko, K. A., Kooshesh, F., Walton, P., McCarthy, J. B., Bissell, M. J., and Turley, E. A. (2006) Rhamm$^{-/-}$ fibroblasts are defective in CD44-mediated ERK1/2 motogenic signaling, leading to defective skin wound repair. *J. Cell Biol.* **175,** 1017–1028 CrossRef Medline
36. Tolg, C., Telmer, P., and Turley, E. (2014) Specific sizes of hyaluronan oligosaccharides stimulate fibroblast migration and excisional wound repair. *PLOS One* **9,** e88479 CrossRef Medline
37. Mohapatra, S., Yang, X., Wright, J. A., Turley, E. A., and Greenberg, A. H. (1996) Soluble hyaluronan receptor RHAMM induces mitotic arrest by suppressing Cdc2 and cyclin B1 expression. *J. Exp. Med.* **183,** 1663–1668 CrossRef Medline
38. Ali, N. J. A., Dias Gomes, M., Bauer, R., Brodesser, S., Niemann, C., and Iden, S. (2016) Essential role of polarity protein Par3 for epidermal homeostasis through regulation of barrier function, keratinocyte differentiation, and stem cell maintenance. *J. Invest. Dermatol.* **136,** 2406–2416 CrossRef Medline
39. Bahrami, S. B., Tolg, C., Peart, T., Symonette, C., Veiseh, M., Umoh, J. U., Holdsworth, D. W., McCarthy, J. B., Luyt, L. G., Bissell, M. J., Yazdani, A., and Turley, E. A. (2017) Receptor for hyaluronan-mediated motility (RHAMM/HMMR) is a novel target for promoting subcutaneous adipogenesis. *Integr. Biol.* **9,** 223–237 CrossRef Medline
40. Stoffels, J. M., Zhao, C., and Baron, W. (2013) Fibronectin in tissue regeneration: timely disassembly of the scaffold is necessary to complete the build. *Cell. Mol. Life Sci.* **70,** 4243–4253 CrossRef Medline
41. Montagner, A., Wahli, W., and Tan, N. S. (2015) Nuclear receptor peroxisome proliferator activated receptor (PPAR) β/δ in skin wound healing and cancer. *Eur. J. Dermatol.* **25,** Suppl. 1, 4–11 CrossRef Medline
42. Sun, Y., Liu, W. Z., Liu, T., Feng, X., Yang, N., and Zhou, H. F. (2015) Signaling pathway of MAPK/ERK in cell proliferation, differentiation, migration, senescence and apoptosis. *J. Recept. Signal Transduct. Res.* **35,** 600–604 CrossRef Medline
43. Tanimura, S., and Takeda, K. (2017) ERK signalling as a regulator of cell motility. *J. Biochem.* **162,** 145–154 CrossRef Medline
44. Haase, I., Evans, R., Pofahl, R., and Watt, F. M. (2003) Regulation of keratinocyte shape, migration and wound epithelialization by IGF-1- and EGF-dependent signalling pathways. *J. Cell Sci.* **116,** 3227–3238 CrossRef Medline
45. Jiang, C., Xu, M., Kuang, X., Xiao, J., Tan, M., Xie, Y., Xiao, Y., Zhao, F., and Wu, Y. (2017) *Treponema pallidum* flagellins stimulate MMP-9 and MMP-13 expression via TLR5 and MAPK/NF-κB signaling pathways in human epidermal keratinocytes. *Exp. Cell Res.* **361,** 46–55 CrossRef Medline
46. Sun, C. K., Man, K., Ng, K. T., Ho, J. W., Lim, Z. X., Cheng, Q., Lo, C. M., Poon, R. T., and Fan, S. T. (2008) Proline-rich tyrosine kinase 2 (Pyk2) promotes proliferation and invasiveness of hepatocellular carcinoma cells through c-Src/ERK activation. *Carcinogenesis* **29,** 2096–2105 CrossRef Medline
47. Sun, C. K., Ng, K. T., Lim, Z. X., Cheng, Q., Lo, C. M., Poon, R. T., Man, K., Wong, N., and Fan, S. T. (2011) Proline-rich tyrosine kinase 2 (Pyk2) promotes cell motility of hepatocellular carcinoma through induction of epithelial to mesenchymal transition. *PLoS One* **6,** e18878 CrossRef Medline
48. Seeger, M. A., and Paller, A. S. (2015) The roles of growth factors in keratinocyte migration. *Adv. Wound Care* **4,** 213–224 CrossRef Medline
49. Tracy, L. E., Minasian, R. A., and Caterson, E. J. (2016) Extracellular matrix and dermal fibroblast function in the healing wound. *Adv. Wound Care* **5,** 119–136 CrossRef Medline
50. Thangavel, C., Boopathi, E., Liu, Y., Haber, A., Ertel, A., Bhardwaj, A., Addya, S., Williams, N., Ciment, S. J., Cotzia, P., Dean, J. L., Snook, A., McNair, C., Price, M., Hernandez, J. R., *et al.* (2017) RB loss promotes prostate cancer metastasis. *Cancer Res.* **77,** 982–995 CrossRef Medline
51. Song, J. M., Molla, K., Anandharaj, A., Cornax, I., O Sullivan, M. G., Kirtane, A. R., Panyam, J., and Kassie, F. (2017) Triptolide suppresses the *in vitro* and *in vivo* growth of lung cancer cells by targeting hyaluronan-CD44/RHAMM signaling. *Oncotarget* **8,** 26927–26940 CrossRef Medline
52. Oldenburg, D., Ru, Y., Weinhaus, B., Cash, S., Theodorescu, D., and Guin, S. (2016) CD44 and RHAMM are essential for rapid growth of bladder cancer driven by loss of glycogen debranching Enzyme (AGL). *BMC Cancer* **16,** 713 CrossRef Medline
53. Klaric, M., Haller, H., Brncic Fischer, A., Babarovic, E., Prijic, A., and Eminovic, S. (2018) The role of CD44 and RHAMM in endometrial (endometrioid type) cancer: an immunohistochemical study. *Appl. Immunohistochem. Mol. Morphol.* **27,** 606–612 CrossRef Medline
54. Ferrer, V. P., Moura Neto, V., and Mentlein, R. (2018) Glioma infiltration and extracellular matrix: key players and modulators. *Glia* **66,** 1542–1565 CrossRef Medline
55. Tammi, M. I., Oikari, S., Pasonen-Seppanen, S., Rilla, K., Auvinen, P., and Tammi, R. H. (2018) Activated hyaluronan metabolism in the tumor matrix–causes and consequences. *Matrix Biol.* **79,** 147–164 CrossRef Medline
56. Barnes, L., Tran, C., Sorg, O., Hotz, R., Grand, D., Carraux, P., Didierjean, L., Stamenkovic, I., Saurat, J. H., and Kaya, G. (2010) Synergistic effect of hyaluronate fragments in retinaldehyde-induced skin hyperplasia which is a Cd44-dependent phenomenon. *PLoS One* **5,** e14372 CrossRef Medline
57. Pasonen-Seppänen, S. M., Maytin, E. V., Törrönen, K. J., Hyttinen, J. M., Hascall, V. C., MacCallum, D. K., Kultti, A. H., Jokela, T. A., Tammi, M. I., and Tammi, R. H. (2008) All-*trans*-retinoic acid-induced hyaluronan production and hyperplasia are partly mediated by EGFR signaling in epidermal keratinocytes. *J. Invest. Dermatol.* **128,** 797–807 CrossRef Medline
58. Porsch, H., Mehić, M., Olofsson, B., Heldin, P., and Heldin, C. H. (2014) Platelet-derived growth factor β-receptor, transforming growth factor β type I receptor, and CD44 protein modulate each other's signaling and stability. *J. Biol. Chem.* **289,** 19747–19757 CrossRef Medline
59. Leng, Y., Abdullah, A., Wendt, M. K., and Calve, S. (2018) Hyaluronic acid, CD44, and RHAMM regulate myoblast behavior during embryogenesis. *Matrix Biol.* **78,** 147–164 CrossRef Medline
60. Tolg, C., McCarthy, J. B., Yazdani, A., and Turley, E. A. (2014) Hyaluronan and RHAMM in wound repair and the "cancerization" of stromal tissues. *Biomed Res. Int.* **2014,** 103923 CrossRef Medline
61. Barnes, L., Ino, F., Jaunin, F., Saurat, J. H., and Kaya, G. (2013) Inhibition of putative hyalurosome platform in keratinocytes as a mechanism for corticosteroid-induced epidermal atrophy. *J. Invest. Dermatol.* **133,** 1017–1026 CrossRef Medline

62. Nylander, N., Smith, L. T., Underwood, R. A., and Piepkorn, M. (1998) Topography of amphiregulin expression in cultured human keratinocytes: colocalization with the epidermal growth factor receptor and CD44. *In Vitro Cell. Dev. Biol. Anim.* **34,** 182–188 CrossRef Medline
63. Herrlich, P., Morrison, H., Sleeman, J., Orian-Rousseau, V., König, H., Weg-Remers, S., and Ponta, H. (2000) CD44 acts both as a growth- and invasiveness-promoting molecule and as a tumor-suppressing cofactor. *Ann. N.Y. Acad. Sci.* **910,** 106–118; discussion 118–20 CrossRef Medline
64. Bourguignon, L. Y. (2014) Matrix hyaluronan-activated CD44 signaling promotes keratinocyte activities and improves abnormal epidermal functions. *Am. J. Pathol.* **184,** 1912–1919 CrossRef Medline
65. Bourguignon, L. Y., and Bikle, D. (2015) Selective hyaluronan-CD44 signaling promotes miRNA-21 expression and interacts with vitamin D function during cutaneous squamous cell carcinomas progression following UV irradiation. *Front. Immunol.* **6,** 224 CrossRef Medline
66. Karousou, E., Misra, S., Ghatak, S., Dobra, K., Götte, M., Vigetti, D., Passi, A., Karamanos, N. K., and Skandalis, S. S. (2017) Roles and targeting of the HAS/hyaluronan/CD44 molecular system in cancer. *Matrix Biol.* **59,** 3–22 CrossRef Medline
67. Hartmann, M., Parra, L. M., Ruschel, A., Böhme, S., Li, Y., Morrison, H., Herrlich, A., and Herrlich, P. (2015) Tumor suppressor NF2 blocks cellular migration by inhibiting ectodomain cleavage of CD44. *Mol. Cancer Res.* **13,** 879–890 CrossRef Medline
68. Senbanjo, L. T., and Chellaiah, M. A. (2017) CD44: a multifunctional cell surface adhesion receptor is a regulator of progression and metastasis of cancer cells. *Front. Cell Dev. Biol.* **5,** 18 CrossRef Medline
69. Yu, Q., and Stamenkovic, I. (1999) Localization of matrix metalloproteinase 9 to the cell surface provides a mechanism for CD44-mediated tumor invasion. *Genes Dev.* **13,** 35–48 CrossRef Medline
70. Chetty, C., Vanamala, S. K., Gondi, C. S., Dinh, D. H., Gujrati, M., and Rao, J. S. (2012) MMP-9 induces CD44 cleavage and CD44 mediated cell migration in glioblastoma xenograft cells. *Cell. Signal.* **24,** 549–559 CrossRef Medline
71. Lawlor, K. T., and Kaur, P. (2015) Dermal contributions to human interfollicular epidermal architecture and self-renewal. *Int. J. Mol. Sci.* **16,** 28098–28107 CrossRef Medline
72. Motegi, S. I., and Ishikawa, O. (2017) Mesenchymal stem cells: the roles and functions in cutaneous wound healing and tumor growth. *J. Dermatol. Sci.* **86,** 83–89 CrossRef Medline
73. Prager, A., Hagenlocher, C., Ott, T., Schambony, A., and Feistel, K. (2017) HMMR mediates anterior neural tube closure and morphogenesis in the frog *Xenopus*. *Dev. Biol.* **430,** 188–201 CrossRef Medline
74. Maxwell, C. A., Benítez, J., Gómez-Baldo, L., Osorio, A., Bonifaci, N., Fernández-Ramires, R., Costes, S. V., Guinó, E., Chen, H., Evans, G. J., Mohan, P., Català, I., Petit, A., Aguilar, H., Villanueva, A., *et al.* (2011) Interplay between BRCA1 and RHAMM regulates epithelial apicobasal polarization and may influence risk of breast cancer. *PLoS Biol.* **9,** e1001199 CrossRef Medline
75. Aragona, M., Dekoninck, S., Rulands, S., Lenglez, S., Mascré, G., Simons, B. D., and Blanpain, C. (2017) Defining stem cell dynamics and migration during wound healing in mouse skin epidermis. *Nat. Commun.* **8,** 14684 CrossRef Medline
76. Zahm, J. M., Kaplan, H., Hérard, A. L., Doriot, F., Pierrot, D., Somelette, P., and Puchelle, E. (1997) Cell migration and proliferation during the *in vitro* wound repair of the respiratory epithelium. *Cell Motil. Cytoskeleton* **37,** 33–43 CrossRef Medline
77. Woodley, D. T., Wysong, A., DeClerck, B., Chen, M., and Li, W. (2015) Keratinocyte migration and a hypothetical new role for extracellular heat shock protein 90α in Orchestrating skin wound healing. *Adv. Wound Care* **4,** 203–212 CrossRef Medline
78. Chen, L., Mirza, R., Kwon, Y., DiPietro, L. A., and Koh, T. J. (2015) The murine excisional wound model: contraction revisited. *Wound Repair Regen.* **23,** 874–877 CrossRef Medline
79. Kobayashi, T., Kim, H., Liu, X., Sugiura, H., Kohyama, T., Fang, Q., Wen, F. Q., Abe, S., Wang, X., Atkinson, J. J., Shipley, J. M., Senior, R. M., and Rennard, S. I. (2014) Matrix metalloproteinase-9 activates TGF-β and stimulates fibroblast contraction of collagen gels. *Am. J. Physiol. Lung Cell Mol. Physiol.* **306,** L1006–L1015 CrossRef Medline
80. Alford, V. M., Kamath, A., Ren, X., Kumar, K., Gan, Q., Awwa, M., Tong, M., Seeliger, M. A., Cao, J., Ojima, I., and Sampson, N. S. (2017) Targeting the hemopexin-like domain of latent matrix metalloproteinase-9 (proMMP-9) with a small molecule inhibitor prevents the formation of focal adhesion junctions. *ACS Chem. Biol.* **12,** 2788–2803 CrossRef Medline
81. Turley, E. A., Wood, D. K., and McCarthy, J. B. (2016) Carcinoma cell hyaluronan as a "portable" cancerized prometastatic microenvironment. *Cancer Res.* **76,** 2507–2512 CrossRef Medline
82. Bourguignon, L. Y. W., Earle, C., and Shiina, M. (2017) Activation of matrix hyaluronan-mediated CD44 signaling, epigenetic regulation and chemoresistance in head and neck cancer stem cells. *Int. J. Mol. Sci.* **18,** E1849 CrossRef Medline
83. Okamoto, I., Kawano, Y., Tsuiki, H., Sasaki, J., Nakao, M., Matsumoto, M., Suga, M., Ando, M., Nakajima, M., and Saya, H. (1999) CD44 cleavage induced by a membrane-associated metalloprotease plays a critical role in tumor cell migration. *Oncogene* **18,** 1435–1446 CrossRef Medline
84. Reiss, K., Ludwig, A., and Saftig, P. (2006) Breaking up the tie: disintegrin-like metalloproteinases as regulators of cell migration in inflammation and invasion. *Pharmacol. Ther.* **111,** 985–1006 CrossRef Medline
85. Miller, M. A., Sullivan, R. J., and Lauffenburger, D. A. (2017) Molecular pathways: receptor ectodomain shedding in treatment, resistance, and monitoring of cancer. *Clin. Cancer Res.* **23,** 623–629 CrossRef Medline
86. Nagano, O., and Saya, H. (2004) Mechanism and biological significance of CD44 cleavage. *Cancer Sci.* **95,** 930–935 CrossRef Medline
87. Chou, C. K., Wu, C. Y., Chen, J. Y., Ng, M. C., Wang, H. M., Chen, J. H., Yuan, S. S., Tsai, E. M., Chang, J. G., and Chiu, C. C. (2015) BubR1 acts as a promoter in cellular motility of human oral squamous cancer cells through regulating MMP-2 and MMP-9. *Int. J. Mol. Sci.* **16,** 15104–15117 CrossRef Medline
88. Mauris, J., Woodward, A. M., Cao, Z., Panjwani, N., and Argüeso, P. (2014) Molecular basis for MMP-9 induction and disruption of epithelial cell-cell contacts by galectin-3. *J. Cell Sci.* **127,** 3141–3148 CrossRef Medline
89. Patruno, A., Ferrone, A., Costantini, E., Franceschelli, S., Pesce, M., Speranza, L., Amerio, P., D'Angelo, C., Felaco, M., Grilli, A., and Reale, M. (2018) Extremely low-frequency electromagnetic fields accelerates wound healing modulating MMP-9 and inflammatory cytokines. *Cell Prolif.* **51,** e12432 CrossRef Medline
90. Shi, Y., Wu, Q., Xuan, W., Feng, X., Wang, F., Tsao, B. P., Zhang, M., and Tan, W. (2018) Transcription factor SOX5 promotes the migration and invasion of fibroblast-like synoviocytes in part by regulating MMP-9 expression in collagen-induced arthritis. *Front. Immunol.* **9,** 749 CrossRef Medline
91. Seomun, Y., Kim, J. T., and Joo, C. K. (2008) MMP-14 mediated MMP-9 expression is involved in TGF-β1-induced keratinocyte migration. *J. Cell. Biochem.* **104,** 934–941 CrossRef Medline
92. Kyriakides, T. R., Wulsin, D., Skokos, E. A., Fleckman, P., Pirrone, A., Shipley, J. M., Senior, R. M., and Bornstein, P. (2009) Mice that lack matrix metalloproteinase-9 display delayed wound healing associated with delayed reepithelization and disordered collagen fibrillogenesis. *Matrix Biol.* **28,** 65–73 CrossRef Medline
93. Ugarte-Berzal, E., Bailón, E., Amigo-Jiménez, I., Albar, J. P., García-Marco, J. A., and García-Pardo, A. (2014) A novel CD44-binding peptide from the pro-matrix metalloproteinase-9 hemopexin domain impairs adhesion and migration of chronic lymphocytic leukemia (CLL) cells. *J. Biol. Chem.* **289,** 15340–15349 CrossRef Medline
94. Dufour, A., Sampson, N. S., Zucker, S., and Cao, J. (2008) Role of the hemopexin domain of matrix metalloproteinases in cell migration. *J. Cell. Physiol.* **217,** 643–651 CrossRef Medline
95. Kouvidi, K., Berdiaki, A., Tzardi, M., Karousou, E., Passi, A., Nikitovic, D., and Tzanakakis, G. N. (2016) Receptor for hyaluronic acid-mediated motility (RHAMM) regulates HT1080 fibrosarcoma cell proliferation via a β-catenin/c-myc signaling axis. *Biochim. Biophys. Acta* **1860,** 814–824 CrossRef Medline
96. Chu, T. L. H., Connell, M., Zhou, L., He, Z., Won, J., Chen, H., Rahavi, S. M. R., Mohan, P., Nemirovsky, O., Fotovati, A., Pujana, M. A., Reid, G. S. D., Nielsen, T. O., Pante, N., and Maxwell, C. A. (2018) Cell cycle-

dependent tumor engraftment and migration are enabled by Aurora-A. *Mol. Cancer Res.* **16,** 16–31 CrossRef Medline
97. Florian, M. C., and Geiger, H. (2010) Concise review: polarity in stem cells, disease, and aging. *Stem Cells* **28,** 1623–1629 CrossRef Medline
98. Shaw, T. J., and Martin, P. (2016) Wound repair: a showcase for cell plasticity and migration. *Curr. Opin. Cell Biol.* **42,** 29–37 CrossRef Medline
99. Entwistle, J., Zhang, S., Yang, B., Wong, C., Li, Q., Hall, C. L., A, J., Mowat, M., Greenberg, A. H., and Turley, E. A. (1995) Characterization of the murine gene encoding the hyaluronan receptor RHAMM. *Gene* **163,** 233–238 CrossRef Medline
100. Tolg, C., Poon, R., Fodde, R., Turley, E. A., and Alman, B. A. (2003) Genetic deletion of receptor for hyaluronan-mediated motility (Rhamm) attenuates the formation of aggressive fibromatosis (desmoid tumor). *Oncogene* **22,** 6873–6882 CrossRef Medline
101. D'Souza, S. J., Pajak, A., Balazsi, K., and Dagnino, L. (2001) Ca^{2+} and BMP-6 signaling regulate E2F during epidermal keratinocyte differentiation. *J. Biol. Chem.* **276,** 23531–23538 CrossRef Medline
102. Morris, V. L., and Chan, B. M. (2007) Interaction of epidermal growth factor, Ca^{2+}, and matrix metalloproteinase-9 in primary keratinocyte migration. *Wound Repair Regen.* **15,** 907–915 CrossRef Medline
103. Yamada, K., Hamashima, T., Ishii, Y., Yamamoto, S., Okuno, N., Yoshida, N., Yamada, M., Huang, T. T., Shioda, N., Tomihara, K., Fujimori, T., Mori, H., Fukunaga, K., Noguchi, M., and Sasahara, M. (2018) Different PDGF receptor dimers drive distinct migration modes of the mouse skin fibroblast. *Cell. Physiol. Biochem.* **51,** 1461–1479 CrossRef Medline